



**HAL**  
open science

## Quantification of diagenetic transformation of continental margin sediments at the Holocene time scale

Céline Charbonnier, Aurélia Mouret, Hélène Howa, Sabine Schmidt, Hervé Gillet, Pierre Anschutz

### ► To cite this version:

Céline Charbonnier, Aurélia Mouret, Hélène Howa, Sabine Schmidt, Hervé Gillet, et al.. Quantification of diagenetic transformation of continental margin sediments at the Holocene time scale. *Continental Shelf Research*, 2019, 180, pp.63-74. 10.1016/j.csr.2019.04.015 . hal-02357287

HAL Id: hal-02357287

<https://hal.science/hal-02357287v1>

Submitted on 22 Oct 2021

**HAL** is a multi-disciplinary open access archive for the deposit and dissemination of scientific research documents, whether they are published or not. The documents may come from teaching and research institutions in France or abroad, or from public or private research centers.

L'archive ouverte pluridisciplinaire **HAL**, est destinée au dépôt et à la diffusion de documents scientifiques de niveau recherche, publiés ou non, émanant des établissements d'enseignement et de recherche français ou étrangers, des laboratoires publics ou privés.



Distributed under a Creative Commons Attribution - NonCommercial 4.0 International License



34 depositional diagenetic processes. Diagenesis of Holocene deposits also contributes to a low,  
35 but significant fraction of N and P flux to the Bay of Biscay sea water.

36

37

38 keywords: Early diagenesis; authigenesis; benthic flux; sediment recording; gravity core; Bay  
39 of Biscay

40

## 41 **1. Introduction**

42

43 Marine sediments are made of partially degraded organic and mineral particles settling  
44 from the water column. Due to permanent supply of settling particles, they are archives of the  
45 evolution of sedimentation conditions. Reconstruction of ocean history from marine  
46 sediments requires to use a wide range of physical, chemical or biological methods and  
47 proxies (Wefer et al., 1999; Calvert and Pedersen, 2007). A proxy is a quantifiable parameter  
48 recorded in the sediment, which allows us to describe a variable that cannot be directly  
49 measured, such as past sea surface temperature, salinity or biological productivity.

50 During the last decades, meter-long piston cores represented the most appropriate  
51 material to reconstruct Quaternary paleo-oceanography. Cores were investigated mainly for  
52 their micropaleontological content and geochemical proxies distribution. Sedimentary  
53 archives recorded in cores are submitted to diagenetic transformations , such as redox  
54 reactions due to organic matter degradation, that can lead to misinterpretation of proxies (e.g.,  
55 Donnadieu et al. 2002; Burdige, 2006; Sundby et al. 2015). The amount of knowledge on  
56 early diagenetic processes is the result of several decades of works, including pioneer studies  
57 of Froelich et al. (1979) on the vertical sequence of redox reactions, Berner (1980) on the  
58 transport-reaction coupling, and Aller (1980) on the influence of macrofauna on  
59 biogeochemical reactions and fluxes. Early diagenetic processes in marine sediments are  
60 driven by the oxidation of naturally occurring organic compounds (La Rowe and Van  
61 Cappellen, 2011) by microorganisms using a sequential series of oxidants in decreasing order  
62 of thermodynamic energy yield (Froelich et al., 1979; De Lange, 1986; Burdige 2006).  
63 Oxygen is the most favourable oxidant, and then nitrate, Mn-oxides and hydroxides, Fe-  
64 oxides and hydroxides, and sulphate are used below the oxic-anoxic boundary. In recent  
65 decades, many works have been published on early diagenetic processes of sediments buried  
66 several metres below the seafloor (e.g. Schulz et al., 1994; Berelson et al., 2005; Chong et al.,

67 2018; Treude et al., 2014; März et al., 2008; Niewohner et al. 1998) – not to speak of the  
68 numerous results on diagenesis in the deep biosphere studied in ODP and IODP drilled cores  
69 (e.g., Arndt et al. 2006, d’Hondt et al. 2004).

70 Diagenesis processes cause chemical gradients and subsequent fluxes of dissolved  
71 chemical compounds that may combine and exchange with the particulate phase. In this way,  
72 properties of the geochemical content buried in the sediment can be modified. Are particularly  
73 concerned proxies such as organic carbon (Reichart et al., 2002), nitrogen (Ganeshram et al.,  
74 1995; Martinez et al., 2000), phosphorus (Ruttenberg and Berner, 1993), transition metals and  
75 trace elements (Chaillou et al., 2002; Calvert and Petersen, 2007), and magnetic signal  
76 (Passier et al., 1998; Garming et al., 2005). Diagenesis processes also affect biological  
77 proxies. Fossilized microorganisms like foraminifera have been intensively used in paleo-  
78 oceanography reconstructions, via their specific characteristics or isotopic chemistry of their  
79 tests (Emiliani, 1955; Berger, 1969; Schiebel et al., 2001). Knowing calcium carbonate  
80 chemistry in marine sediments is essential to calibrate these calcareous micropaleontological  
81 proxies and to understand eventual changes in the geochemical properties of their shell during  
82 burial (Dittert et al., 1999).

83 Early diagenesis processes in the Bay of Biscay slope have been investigated from  
84 interface cores (~20 to 50 cm-long) during the last twenty years. Studies focused on suboxic  
85 diagenesis (Hyacinthe et al., 2001), benthic foraminifera micro-environments (Fontanier et al.,  
86 2002), trace metal diagenesis (Chaillou et al., 2002), effects of turbiditic layers (Anschutz et  
87 al., 2002; Chaillou et al., 2008), benthic manganese geochemistry (Mouret et al., 2009), and  
88 oxygen and organic carbon fluxes in upper sediment (Mouret et al., 2010). Completing these  
89 results on the upper sedimentary layer, piston cores over 1 to 3 m in length have been  
90 collected and analysed in order to characterize anoxic diagenetic processes in Holocene  
91 sediments. Beyond the regional relevance of our results, the aim of the present study was to  
92 determine how redox reactions linked to organic matter mineralization could change sediment  
93 chemistry, and how a recorded signal could be modified in the almost steady state situation of  
94 the Holocene. In this purpose, we measured a large range of particulate and pore water  
95 compounds involved in early diagenesis reactions in order to determine geochemical  
96 transformations from mass balance calculations based on flux estimates. This data set also  
97 allowed us to assess fluxes of nutrient to the sediment surface due to deep diagenesis  
98 processes.

99

## 100 **2. Material and methods**

101

### 102 **2.1. Study area**

103

104 The Bay of Biscay is located on the eastern side of the Northern Atlantic Ocean, bathed  
105 by oceanic waters from the North Atlantic Drift. Several rivers in France and Spain feed the  
106 sedimentary basin. The Gironde estuary and the Loire River are presently the main sources of  
107 fresh water and fine sediments to the margin (Borja et al., 2019). The four stations sampled  
108 (D, B, A and WH, Fig. 1) have been chosen according to a bathymetric transect from 150 to  
109 2000 m water depth on the continental slope of the Landes Plateau. Stations at 150 m (D) and  
110 550 m (B) water depth are under the influence of North Atlantic Central Waters (about 10-  
111 12°C), whereas station A at 1000 m water depth is under the influence of Mediterranean  
112 Ocean Waters (about 10°C) and station WH at 2000 m water depth is under the influence of  
113 North Atlantic Deep Waters (Anschutz and Chaillou, 2009). Sediment consists of mud  
114 composed of siliciclastic clay and silt, and 15 to 35 dw% (dry weight percent) of carbonates  
115 (Hyacinthe et al., 2001). Sediment accumulation rates (SAR) were inferred from  $^{210}\text{Pb}_{\text{xs}}$  (half-  
116 life=22.3 years) activity profiles, sediment porosity, and a model based on steady-state  
117 manganese diagenesis (Chaillou et al., 2002; Mouret et al., 2009). SAR decreases offshore,  
118 from 50 – 80  $\text{mg cm}^{-2} \text{yr}^{-1}$  at station B, about 35  $\text{mg cm}^{-2} \text{yr}^{-1}$  at station A to about 10  $\text{mg cm}^{-2}$   
119  $\text{yr}^{-1}$  at station WH. At the shallowest station D,  $^{210}\text{Pb}$  profiles indicate a maximal rate around  
120 1630  $\text{mg cm}^{-2} \text{yr}^{-1}$ , but this value should not be considered according to high bioturbation  
121 thickness observed in the upper part of the core (Schmidt et al., 2009). Additional data  
122 presented in this paper allowed us to better constraint SAR in the Bay of Biscay. Following  
123 Mouret et al. (2010), the mean depth of dissolved oxygen penetration was 6 mm at station D,  
124 2 cm at station B, 3.2 cm at station A, and 6 cm at station WH.

125

### 126 **2.2. Sampling and sample processing**

127

128 Depending on the four stations, the upper sediment was sampled 4 to 16 times between  
129 1997 and 2009, with an interface multi-corer. Samplings were achieved during OXYBENT,  
130 FORAMPROX and PECH cruises on board the RV “Côtes de la Manche”. The multi-corer  
131 allows sampling the upper few decimetres of sediments, the overlying bottom waters, and the  
132 undisturbed sediment-water interface, in a 10 cm diameter Plexiglas tube. At a given station,  
133 very similar profiles of redox reactive compounds were measured in all short cores collected

134 during 10 years (Mouret et al., 2016). Only light differences were noticed at the sediment  
135 surface, which were attributed to seasonality, bioturbation, or patchiness.

136

137 One to 3.5 meter long Kullenberg cores were collected in duplicate at the four stations  
138 during the PROSECAN IV cruise organized in May 2007 onboard the RV “Thallia” and the  
139 CADIAC1 and 2 (June and August 2009) cruises on board the RV “Côtes de la Manche”. For  
140 each station, one core was sealed for later sedimentary analyses, and micropaleontological  
141 studies (Mojtahid et al., 2013; Garcia et al., 2013). The second core was immediately sub-  
142 sampled on board for biogeochemical analyses and  $^{14}\text{C}$  dating. Two cm thick horizontal  
143 sections were cut with a sampling step between 5 and 20 centimetres. For each level, a  $\sim 5\text{ cm}^3$   
144 sub-sample was immediately sealed in a pre-weighted vial, and frozen for further  
145 determination of porosity and analyses of the solid fraction. Another sub-sample was  
146 centrifuged on board under inert  $\text{N}_2$ -atmosphere at 4000 rpm for 15 minutes in order to collect  
147 pore waters. Supernatant was filtered ( $0.2\ \mu\text{m}$  cellulose acetate syringe filter). An aliquot was  
148 frozen for inorganic nitrogen compound analyses, a second aliquot was acidified with  
149 ultrapure HCl for dissolved phosphate, Mn, and Fe analyses. During the CADIAC cruises,  
150 sampling was realized for pore water methane analyses:  $5\text{ cm}^3$  sediment was sealed in a pre-  
151 weighted glass vial with 1 mL 1M NaOH.

152

### 153 **2.3. Analyses**

154

155 Grain size was measured every 5 cm using a laser diffractometer Malvern Mastersize. A  
156 1 cm thick slab was sampled along the core length and X-radiographed using the Scopix  
157 system (Migeon et al., 1999), which consists of an X-ray imaging system combined with  
158 image analysis software.

159 Three or four sediment sub-samples were collected along the cores and sieved through  
160  $150\text{-}\mu\text{m}$  mesh screen for foraminifera picking. Radiocarbon dating was performed by UMS-  
161 ARTEMIS (Pelletron 3MV) AMS facilities (CNRS-CEA Saclay, France) on hand-picked  
162 *Globigerina bulloides*, *Neogloboquadrina pachyderma* or on the bulk planktic foraminifera  
163 assemblage, according to the microfauna of each sample. The  $^{14}\text{C}$  age ( $^{14}\text{C}$  yr BP) was  
164 converted to calendar age (cal yr BP) using the Fairbanks program version 0107 (Fairbanks et  
165 al., 2005) taking into account a reservoir age of 400 years.

166 Maximum sediment mass accumulation rate of station D core was estimated from  
167 profiles of  $^{210}\text{Pb}_{\text{xs}}$  with depth. Activities of  $^{210}\text{Pb}$  and of its radioactive parent,  $^{226}\text{Ra}$ , were

168 determined in about 4–6 g of freeze-dried material sealed in a counting vial, by high-  
169 resolution and low-background gamma spectrometry for 4–24 h (Jouanneau et al. 1998;  
170 Schmidt et al. 2007). The  $\gamma$  detectors were calibrated with IAEA RGU-1 reference materials.  
171 Supported  $^{210}\text{Pb}$  was obtained from  $^{214}\text{Bi}$  and  $^{214}\text{Pb}$  peaks. By subtracting the activity of  $^{226}\text{Ra}$   
172 from the  $^{210}\text{Pb}$  total specific activity, we obtained the unsupported  $^{210}\text{Pb}$  component, and we  
173 used it to determine accumulation rates. The gamma spectra of samples also gave the  $^{137}\text{Cs}$   
174 activity, which was useful for core D to determine the modern sediment layer deposited for  
175 the last 60 years.

176 Porosity was calculated from particle density and water content determined by  
177 comparison of the weights of wet and dried (lyophilised) sediment. Particle density was  
178 estimated at 2.65 (Berner, 1980), which is the mean density of alumino-silicate and calcium  
179 carbonate minerals. The dried solid fraction was homogenized and water content was used to  
180 correct analyses for the presence of sea salt that precipitated during lyophilisation. Particulate  
181 sulphur and total carbon were measured on the freeze-dried sediment by infrared spectroscopy  
182 using a LECO C/S 200. Particulate organic carbon (POC) concentration was measured with  
183 the same method after removal of carbonates with 2N HCl from 50 mg of powdered sample  
184 (Etcheber et al., 1999). Particulate inorganic carbon is the difference between total and  
185 organic carbon. In core WH, because of the presence of 2N HCl refractory carbonates,  
186 carbonate content was measured by a calcimetric method. Particulate organic carbon was then  
187 deduced by the difference with the total carbon. Solid-phase samples were subjected to two  
188 different extraction techniques for determination of reactive solid-phase Mn and Fe. The most  
189 reducible fraction (Fe-asc and Mn-asc) was extracted with an ascorbate solution buffered at  
190 pH 8 (Anschutz et al., 2005). A second extraction on a separate aliquot was carried out with  
191 1N HCl to determine acid soluble Mn (Mn-HCl) and Fe (Fe-HCl). For ascorbate and 1N HCl  
192 procedures, about 100 mg dried sample was leached with 10 mL of solution during 24-h while  
193 shaking continuously at ambient temperature. The supernatant was diluted ten times with  
194 0.2N HCl for ascorbate extraction, and with water for HCl extraction. Mn-HCl represents the  
195 whole fraction of Mn-oxides and Mn associated with carbonates. Mn-asc represents the major  
196 part of reducible Mn (III, IV) oxides and oxyhydroxides. Iron extracted with HCl comes from  
197 the fraction extracted by ascorbate, FeS, some iron phyllosilicates and carbonates. Phosphorus  
198 was also measured in leaching solutions. P extracted with ascorbate (P-asc) derives from P  
199 associated with Fe-oxides extracted with ascorbate (Anschutz et al., 1998). P extracted with  
200 HCl represents inorganic particulate P, i.e. P associated with iron oxides, carbonates and  
201 lithogenic and authigenic phosphate minerals (Ruttenberg, 1992).

202 Pore water compounds were analysed using techniques adapted for small volumes of  
203 samples. Nitrate was measured by flow injection analysis (FIA) according to Anderson  
204 (1979). Ammonium and dissolved inorganic carbon (DIC) were analysed with the FIA method  
205 described by Hall and Aller (1992). Sulphate was measured with a nephelometric method  
206 using BaCl<sub>2</sub>, and Fe<sup>2+</sup> with the colorimetric method using ferrozine (Stookey, 1970).  
207 Phosphate in pore water and in leaching solutions was measured by a colorimetric method  
208 according to Anschutz and Deborde (2016). Manganese was measured by flame atomic  
209 absorption spectrometry (FAAS, Perkin Elmer AA 300) using an external aqueous standard  
210 for calibration. Calcium was also determined by FAAS using Lanthanum chloride as matrix  
211 modifier (Haswell, 1991). Methane was measured using a gas chromatograph (Hewlett  
212 Packard HP 5890A). The reproducibility of analyses was better than 5%.

213

### 214 **3. Results**

215

#### 216 **3.1. Sedimentary and biostratigraphic observations**

217

218 The sediment-water interface was well preserved in interface cores collected with the  
219 multi-corer, whereas the upper centimetres of sediment from the Kullenberg cores were lost.  
220 To estimate this sediment loss in cores used for biogeochemical analyses, we compared the  
221 profiles of reactive compounds, such as ammonium, dissolved Mn and Mn-asc, or the  
222 porosity profiles measured in the Kullenberg cores with profiles from the interface cores. In  
223 this way, we were able to correct the vertical scale, with a precision of ±1 cm. All depths cited  
224 here are corrected depths. Core taken in duplicate at each site for sedimentological and  
225 micropaleontological analyses

226 X-ray images showed a clay/silty-clay facies for all studied sites. At station D, muds  
227 were dark brown down to 133 cm and became black below. The mean grain size of particles  
228 was between 10 and 15 µm (Fig. 2). At the deeper station B, sediment also showed moderate  
229 grain size variations. The mean grain size of particles was 10 µm in the upper 20 cm. It was  
230 between 10 and 15 µm down to 3 m depth, and reached at 18 µm at the bottom. At station A,  
231 sediment was silty clay except between 60 and 80 cm depth, where a silty sand facies  
232 occurred. The mean grain size of the sediment particles was around 5-6 µm in the clay facies  
233 and reached 35 µm in the silty sand layer. At the 2000 m depth station WH, the sediment was  
234 quite homogeneous along the core, with a mean grain size around 6 µm. Histograms of grain

235 size frequency have been realized for all stations. They indicate an unimodal distribution with  
236 a major mode between 6 and 10  $\mu\text{m}$  depending on the stations. Two discreet secondary modes  
237 at 30-40  $\mu\text{m}$  and 200  $\mu\text{m}$  can be observed and are attributed to silt and fossilized foraminifera  
238 fraction, respectively.

239 Radiocarbon measurements along the cores gave ages between  $173\pm 92$  and  $16437\pm 128$   
240 cal years. Core WH and A recorded the entire Holocene period within less than 1 m. The  
241 beginning of the Holocene corresponded to the silty-sand facies between 60 and 80 cm depth  
242 in core A. At station B, the 320 cm long core contained Holocene sediment, since an age of  
243  $8990\pm 32$  cal years measured at 280 cm depth. Sediments of the shallow core D gave  
244 inconsistent  $^{14}\text{C}$  ages. The presence of detectable  $^{210}\text{Pb}_{\text{xs}}$  levels at 96 cm depth, and the  
245 occurrence of the man-generated  $^{137}\text{Cs}$  isotope at 56 cm depth showed that the 2 m long core  
246 D contained modern sediments. The  $^{210}\text{Pb}_{\text{xs}}$  activity decreased with a slope that corresponds  
247 to a sedimentation rate of  $0.76 \text{ cm yr}^{-1}$ . The mass accumulation rate, deduced from the  
248 sedimentation rate and the cumulated particle mass deduced from the porosity gradient, was  
249  $0.63 \text{ g cm}^{-2} \text{ yr}^{-1}$ , suggesting a deposition of the bottom sediment of the core D 270 years  
250 before sampling.

251 At stations D, B, WH and the first 80 cm of station A core, planktic foraminifera  
252 assemblage was composed by a typical fauna of subtropical/temperate areas (*Globigerina*  
253 *bulloides*, *Orbulina sp.*, *Globorotalia truncatulinoides* (sinistral)). The high abundance of  
254 *Turborotalia humilis*, which is only observed during the Holocene period in the Bay of  
255 Biscay, indicated that the time period sampled was less than 10 000 years, in agreement with  
256  $^{14}\text{C}$  dating. In the core A, planktic foraminifera assemblage below 113 cm depth was  
257 dominated by the subpolar/polar species *Neogloboquadrina pachyderma*.

258

### 259 **3.2. Reactive solid fraction**

260

261 Particulate organic carbon content was between 2.2 dw% and 1 dw% in surficial  
262 sediments (Fig. 3). The highest values were measured in the shallowest station cores (D and  
263 B). POC content decreased with core depth, and at 1 m depth it reached 1.4 dw% at station D,  
264 0.8 dw% at station B, 0.4 dw% at station A, and 0.5 dw% at station WH (Fig. 3). For all sites,  
265 particulate sulphur values increased with core depth. In the first centimetre, particulate  
266 sulphur concentrations remained close to  $10 \mu\text{mol g}^{-1}$  and reached at 120 cm depth  $70 \mu\text{mol g}^{-1}$   
267 at station B,  $32 \mu\text{mol g}^{-1}$  at station A, and  $55 \mu\text{mol g}^{-1}$  at station WH. At station D,  
268 particulate sulphur values reached  $100 \mu\text{mol g}^{-1}$  within 20 cm and reached a maximum of 189

269  $\mu\text{mol g}^{-1}$  at 176 cm depth, in the dark zone of the sediment. For a given station, HCl and  
270 ascorbate extractions showed vertical profiles with similar shapes, but HCl extraction were  
271 more concentrated in Fe, Mn and P than ascorbate extractions. Profiles showed a subsurface  
272 maximum, and quite constant and lower values below. At station D, extracted Fe and P values  
273 increased at around 130 cm depth and remained steady below (Fig. 4).

274 At stations A and B, Mn-asc and P-asc values remained low in the anoxic zone, whereas  
275 Mn-HCl and P-HCl, increased slightly with core depth (Fig. 4). Mean particulate inorganic  
276 carbon concentrations increased with the water depth, ranging from 2 dw% at station D to 4  
277 dw% at station WH. The corresponding  $\text{CaCO}_3$  content varied between 16 and 33 dw%,  
278 respectively (Fig. 3). At station A,  $\text{CaCO}_3$  concentration of Holocene sediment was twice the  
279 concentrations measured downcore below 80 cm (pre-Holocene sediments).

280

### 281 **3.3. Pore water composition**

282

283 The pore space, that defined the porosity ( $\Phi$ ), showed a logarithmic decrease downcore  
284 (Fig. 2). Between the surface and 1 m depth, porosity decreased from 0.86 to 0.67 at station  
285 D, from 0.85 to 0.57 at station B, from 0.84 to 0.61 at station A and from 0.86 to 0.62 at  
286 station WH. A minimal value of 0.55 at 68 cm depth was observed in core A, corresponding to  
287 the silty sand zone.

288 Dissolved redox compounds showed the well established distribution (Froelich et al.,  
289 1979), in which oxic compounds, such as nitrate and sulphate, decreased with depth (Fig. 5),  
290 and reduced compounds, such as dissolved iron, manganese, and ammonia were below or  
291 close to the detection limit in the oxic layer, and their concentrations increased below.  
292 Recycled compounds, as dissolved inorganic phosphorus (DIP) and DIC increased with depth  
293 (Fig. 5). More precisely, bottom water concentrations of nitrate increased with water depth  
294 from 4  $\mu\text{M}$  at station D to 33  $\mu\text{M}$  at station WH. Nitrate concentration decreased steeply  
295 below the sediment-water interface, but concentrations always remained above the detection  
296 limit in the anoxic part of the sediment column, between 1 and 5  $\mu\text{M}$ . Sulphate remained close  
297 to sea water concentration at the top of the cores. Downcore profiles indicated a slight  
298 decrease at the deeper stations (A and WH), with respective values of 29 and 25 mM at 110  
299 cm depth. At station B, sulphate decline was stronger, with a concentration of 10 mM at 210  
300 cm depth. At station D, sulphate were completely consumed, with values below detection  
301 limit below 160 cm depth. Recycled compound concentrations, such as ammonia, DIC and  
302 DIP, increased more sharply at the shallower stations (D and B) than at deeper stations (A and

303 WH). These concentrations remained close to sea water concentrations at the surface  
304 sediment, and then they increased with depth. So, ammonia concentrations at 1 m depth  
305 reached 2000  $\mu\text{M}$  in core D, 1500  $\mu\text{M}$  in core B, 164  $\mu\text{M}$  in core A and 390  $\mu\text{M}$  in core WH.  
306 Respective concentrations of DIC at the same depth were 15 mM, 9 mM, 3.0 mM and 2.2 mM  
307 whereas DIP concentrations reached 20  $\mu\text{M}$ , 19.7  $\mu\text{M}$ , 2.5  $\mu\text{M}$  and 6.5  $\mu\text{M}$ , respectively.  
308 Reduced dissolved compounds, as iron, manganese and sulphides, were observable all along  
309 the Kullenberg cores. Dissolved iron concentrations showed maximal values at the top of the  
310 cores just below the oxic layer (between 30 to 120  $\mu\text{M}$ ), then decreased and became lower  
311 than 10  $\mu\text{M}$  at depth, except at station D, where concentrations increased again down to 200  
312 cm depth and reach 30.6  $\mu\text{M}$  at 196 cm depth. Dissolved manganese concentrations increased  
313 in the first decimetres of sediments, with a maximum at 2 cm depth at station D, 8.5 cm depth  
314 at station B, 18 cm depth at station A and 25 cm depth at station WH. Deeper in the sediment,  
315 dissolved manganese concentration decreased to values less than 10  $\mu\text{M}$  below 1 m depth.  
316 Dissolved calcium concentrations were close to the sea water value of 10.5 mM at the top of  
317 sediment cores and decreased steadily with depth. The higher gradient was observed at station  
318 D, where values reached 1.75 mM at the bottom of the 2 m-long core. Pore water methane  
319 concentration had constant and low values for all samples, except below 150 cm depth at  
320 station D (584  $\mu\text{M}$  at 178 cm depth and 366  $\mu\text{M}$  at the bottom of the core, Fig. 5).

321 To summarize, station D is characterized by quite large organic matter concentrations  
322 (>2%), a weak oxygen penetration depth and a complete consumption of sulphate at 150 cm  
323 depth. Downcore, methane concentrations increase strongly. Dissolved compounds directly  
324 produced by organic matter mineralization increase with depth, whereas dissolved manganese  
325 and calcium concentrations decrease. Station B shows moderate organic carbon  
326 concentrations (POC = 1.9% at the surface sediment), dissolved oxygen penetrates deeper in  
327 the sediment (2 cm) and a significant sulphate decreasing gradient occurs, even if sulphate is  
328 not completely consumed downcore. The same trends are observed for recycled dissolved  
329 compounds and dissolved manganese and calcium. Station A is characterized by quite weak  
330 POC contents (POC = 1% at the core top), a dissolved oxygen penetration depth of 3.2 cm  
331 and the presence of the Holocene-Pleistocene transition between 60 and 80 cm depth. This  
332 transition layer is observable on some profiles, with an increase in ascorbate and HCl  
333 extracted phosphorus, manganese and iron (Fig. 4), and a decrease in POC and carbonate  
334 concentrations (Fig. 3). However, ammonia, DIP and DIC concentrations increase regularly  
335 with depth and sulphate and dissolved calcium values decrease slightly. Dissolved manganese  
336 profile shows a strong decrease with depth. Station WH is characterized by a POC content

337 less than 1.5% at the core top, and a dissolved oxygen penetration depth of 6 cm. Recycled  
338 dissolved compounds, sulphate, dissolved calcium and manganese profiles show similar  
339 trends than at station A.

340

## 341 **4. Discussion**

342

### 343 **4.1. Sediment accumulation rate**

344

345 Sedimentation appears to remain steady throughout the Holocene period, since no  
346 interruption of sediment structure could be observed, and the profiles of reactive particulate  
347 compounds, as POC or Fe and Mn content from HCl leaching show a regular shape. The 3 m-  
348 long core B and the 1.25 m-long core WH have recorded the Holocene period, with  $^{14}\text{C}$  ages  
349 at the bottom of the cores of  $8982\pm 32$  and  $12113\pm 67$  cal years BP respectively (Fig. 2). At  
350 station A, Holocene deposits constitute the top 70 cm of the core ( $11230\pm 20$  cal years BP at  
351 73 cm depth), and the end of the last glacial period is recorded downcore with a radiocarbon  
352 age of  $16437\pm 128$  cal years BP determined at 161 cm depth. The transition between these two  
353 periods is marked by a silty sand layer, probably due to strong fluvial discharges linked to  
354 European ice sheet melting (Eynaud et al., 2007). Dissolved element concentrations do not  
355 show any change around this transition, because past gradients are smoothed by molecular  
356 diffusion (DeLange, 1983). At station D,  $^{210}\text{Pb}$  data of the top meter of sediment suggest  
357 that the entire sedimentary column at site D has been deposited during the last 270 years.

358 In the Holocene sequence in the Bay of Biscay, carbonates consist mainly of marine  
359 microorganism remains (Garcia et al., 2013). Carbonate content is quite constant at a given  
360 site. However, an obvious offshore-onshore gradient occurs with values around 35% at the  
361 deepest stations (A and WH), more than 20% at station B and 12% at station D (Fig. 3). The  
362 shallowest site D is under continental influence with sedimentation dominated by silicoclastic  
363 supplies that decline offshore supplanted by bio-production of carbonates.

364 Porosity data allow us to integrate the inventory of particles over the whole length of the  
365 long cores. Considering a mean particle density of 2.65 (Berner, 1980) and an horizontal  
366 section of  $1\text{ cm}^2$ , this inventory is about 182 g from the top to the bottom of core D, 360 g in  
367 core B, 65.5 g in the Holocene sequence of core A and 103 g in core WH. Using the  $^{14}\text{C}$   
368 dating recorded at the bottom of the cores, we obtain that the mean mass accumulation rate  
369 (MAR) is  $40\text{ mg cm}^{-2}\text{ yr}^{-1}$  at station B,  $5.8\text{ mg cm}^{-2}\text{ yr}^{-1}$  in the Holocene period of station A

370 and 8.5 mg cm<sup>-2</sup> yr<sup>-1</sup> at station WH. At station D, <sup>210</sup>Pb<sub>xs</sub> data give a MAR of 630 mg cm<sup>-2</sup> yr<sup>-1</sup>. Values of MAR inferred from our core analysis, integrating long-term sedimentation, can be  
371 compared with results obtained from surface sediment data, as <sup>210</sup>Pb<sub>xs</sub> dating, ages deduced  
372 from the Mn diagenesis model (Mouret et al., 2009), or mass fluxes calculated from sediment  
373 traps deployed in the water column (Schmidt et al., 2009). At station B, fluxes deduced from  
374 <sup>14</sup>C dating are about two times lower than results from surface methods (50 to 80 mg cm<sup>-2</sup> yr<sup>-1</sup>);  
375 at station A, MAR from <sup>14</sup>C dating is about one order of magnitude lower compared to  
376 other methods (35 mg cm<sup>-2</sup> yr<sup>-1</sup>). At station WH, all methods give exactly the same results.  
377 Such discrepancy at stations B and A suggests that dating and deduced mass fluxes based on  
378 methods used in surface sediment are affected by surface processes. For instance, <sup>210</sup>Pb<sub>xs</sub>  
379 dating of station WH, A and B was most probably overestimated in previous studies because  
380 of bioturbation-induced particle mixing in the upper part of the sediment column (Soetaert et  
381 al., 1996). Except station D, radiocarbon ages can be considered as the most confident date to  
382 calculate mean MAR in Holocene sediments because they are acquired far below the  
383 bioturbation zone.  
384

385

386

#### 387 **4.2. Diagenetic sequence**

388

389 Interface core data show that oxygen concentrations decrease rapidly below the  
390 sediment-water interface (Mouret et al., 2010). Nitrate strongly decreases below the layer that  
391 contains oxygen. The disappearance of oxygen and nitrate goes along with a decline of the  
392 Mn-oxides and Fe-oxides content and an increase in dissolved manganese and iron. Deeper  
393 down the Kullenberg long cores, sulphate content decreases linearly. At station D, sulphate is  
394 totally consumed and high methane concentrations appear at the bottom of the core, where  
395 there is no more sulphate. This distribution follows the well-established depth sequence of  
396 diagenetic reactions governed by the preferential use of the electron acceptor that yields the  
397 highest amount of free energy for the bacterially mediated oxidation of organic matter  
398 (Froelich et al., 1979; Postma and Jacobsen, 1996). In the following discussion we will  
399 attempt to quantify processes, in which reactive compounds are involved in the Holocene  
400 anoxic sediment and estimate the consequent implications for interpretation of sedimentary  
401 record.

402

403 Previous works on dissolved oxygen profiles at the studied stations have shown that the  
quantity of carbon mineralized by oxic processes is above POC content in the surficial

404 sediment (Mouret et al., 2010). It has been proved that POC measured in surficial sediment at  
405 stations B, A and WH are remains that represented respectively only 45%, 25% and 15% of  
406 settling carbon, the other part being rapidly mineralized through aerobic processes at the  
407 sediment-water interface.

408 The rapid decrease in organic matter content in the upper centimetres of the sediment  
409 and the profiles of redox compounds indicate that organic matter mineralization rates are  
410 highest near the sediment-water interface. The occurrence of linear pore water profiles and  
411 almost constant POC, Fe-asc and Mn-asc values below this reactive zone imply the existence  
412 of an intermediate reaction-poor, diffusion-dominated zone. The almost linear decrease in  
413 sulphate concentration suggests that a reaction zone occurs at depth. At station D, the  
414 consumption of sulphate is associated with the transition between sulphate reduction and  
415 methane-bearing sediments. This has been observed in many continental margin sediments.  
416 Sulphate concentrations go to zero as methane diffuses upward where it is oxidized by  
417 sulphate through a microbial process of anaerobic oxidation of methane (AOM) (Martens and  
418 Berner, 1974; Nauhaus et al., 2002 ; Reeburgh, 2007; Knittel and Boetius, 2009). In cores B,  
419 A, and WH, the transition zone between sulphate and methane was not observed, probably  
420 because it occurred just below (B) or far below (A and WH) the bottom of the collected cores.  
421 The depth of the transition zone may vary from less than a meter below the sediment surface  
422 to several tens of metres in different settings (e.g., Iversen and Jørgensen, 1985; Borowski et  
423 al., 1999; Dickens, 2001; D'Hondt et al., 2004; Hensen et al., 2003; Berelson et al., 2005;  
424 Snyder et al., 2007; März et al., 2008). The depth of methane production zone is probably  
425 linked to the evolution of a parameter that allows the refractory fraction of organic matter to  
426 become reactive at depth. Burdige (2011) suggested that the geothermal gradient could be the  
427 physical parameter that explained that refractory material becomes more reactive with depth  
428 due to increasing temperature. In continental margin sediments, immense sub-surface  
429 accumulations of methane can be present in the form of methane hydrate (e.g. Bohrmann and  
430 Torres, 2006; Ruppel and Kessler, 2017). Methane hydrate have not been evidenced until now  
431 in the southern Bay of Biscay, but emission of gas at the seafloor issuing from sub-surface  
432 methane have been observed recently (Dupré et al., 2014 ; Pierre et al., 2017 ; Ruffine et al.,  
433 2017).

434 Profiles of dissolved sulphate are almost linear. A slight curvature occurs at station B.  
435 This can be due to a decrease in porosity with depth and a resulting decrease in diffusion  
436 coefficient (Boudreau, 1996). The curvature can be directly linked to sulphate reduction  
437 through anaerobic oxidation of organic matter within the layer located above the sulphate-

438 methane transition zone. Even if the curvature of the profile is not obvious in the studied  
439 stations, the increasing concentration of particulate sulphur with depth suggests that sulphate  
440 reduction does occur along the studied cores. Moreover, model results (Burdige et al., 2016)  
441 show that linear profiles may also occur when high rates of sulphate reduction occur near the  
442 sediment surface and at the sulphate-methane transition zone with low, but nonzero, rates of  
443 sulphate reduction in between. At the same time, linearity in the sulphate profile may also be  
444 related to downward pore-water advection by compaction and sedimentation (Burdige et al.,  
445 2016). A flux of dissolved sulphate to the sediment can be calculated and then a rate of  
446 organic matter mineralization through sulphate-reduction can be deduced according to the  
447 stoichiometry of the reaction (two carbons for one sulphate; Burdige, 2006). The flux of  
448 dissolved compounds in pore waters in steady state conditions was calculated considering the  
449 vertical distribution of the dissolved compound and porosity gradient within the sediment,  
450 according to Fick's first law of diffusion (Schulz and Zabel, 2006):

451

$$452 \quad J = - \Phi D_s dC/dX$$

453

454 where  $J$  is the flux,  $\Phi$  is the porosity,  $dC/dX$  is the concentration gradient, and  $D_s$  is the  
455 bulk sediment molecular diffusion coefficient, assumed to be equal to  $D_s = D_o / [1 - \ln(\Phi^2)]$   
456 (Boudreau, 1996), where  $D_o$  is the diffusion coefficient in water at *in situ* temperature (Schulz  
457 and Zabel, 2006). Bioturbation and bioirrigation processes have been neglected in the flux  
458 model since most diffusive processes discussed here concern sediment depth located below  
459 the surface layer affected by these processes. The calculated flux of dissolved sulphate is 18.1  
460  $\mu\text{mol cm}^{-2} \text{ yr}^{-1}$  at station D, 4.3  $\mu\text{mol cm}^{-2} \text{ yr}^{-1}$  at station B, 0.48  $\mu\text{mol cm}^{-2} \text{ yr}^{-1}$  at station A,  
461 and 1.26  $\mu\text{mol cm}^{-2} \text{ yr}^{-1}$  at station WH (Table 1). These values correspond to rates of POC  
462 mineralization of 36.3, 8.5, 1.0, and 2.5  $\mu\text{mol cm}^{-2} \text{ yr}^{-1}$ , respectively.

463

464 Similar calculations can be realized based on ammonia fluxes in order to assess  
465 mineralization processes that occur in buried sediments (Soetaert et al., 1996; Burdige and  
466 Komada, 2013). Fluxes of  $\text{NH}_4^+$  obtained (Table 1) are 4.49  $\mu\text{mol cm}^{-2} \text{ yr}^{-1}$  at station D, 1.25  
467  $\mu\text{mol cm}^{-2} \text{ yr}^{-1}$  at station B, 0.18  $\mu\text{mol cm}^{-2} \text{ yr}^{-1}$  at station A and 0.41  $\mu\text{mol cm}^{-2} \text{ yr}^{-1}$  at station  
468 WH. Considering a typical C:N ratio of marine organic matter of 106:16 (Redfield et al.,  
469 1963), these values correspond to POC mineralization rate of 29.7, 8.3, 1.2 and 2.7  $\mu\text{mol cm}^{-2}$   
470  $\text{yr}^{-1}$ , respectively. These values are close to organic carbon mineralization rates deduced from  
471 sulphate profiles. This should not be considered as an indication that dissimilatory sulphate  
reduction is the only process of N mineralization during anoxic diagenesis, because

472 methanogenesis produces ammonium as well. When sulphate is reduced with methane, one  
473 methane reacts with one sulphate. As 16:53 ammonium is produced for one methane produced  
474 during methanogenesis, and also for one sulphate consumed during sulphate reduction,  
475 according to a Redfield composition of organic matter (C:N=106:16), the production of  
476 ammonium relative to sulphate consumption remains the same whatever the process for  
477 sulphate reduction (AOM or dissimilatory).

478         Considering that chemical fluxes and MAR are steady during the Holocene, it is  
479 possible to calculate the loss of POC due to organic matter mineralization by anoxic processes  
480 that consume sulphate. Calculated values are 0.058, 0.21, 0.16 and 0.30 mmol of mineralized  
481 POC per gram of dry sediment, at stations D, B, A, and WH respectively, which represent  
482 0.69, 2.6, 2.0 and 3.6 mgC g<sup>-1</sup>. It corresponds to a decrease in POC concentration of 0.069%  
483 (D), 0.26% (B), 0.2% (A) and 0.36% (WH) by sulphate reduction and methanogenesis. We  
484 observe a decrease in POC concentration in the anoxic part of studied cores, although POC  
485 loss is lower than that calculated above. This is probably because our long cores have only  
486 sampled the upper part of the anoxic zone. More particularly, Kullenberg cores B, A, and WH  
487 did not sample the deep sediment zone in which sulphate disappears. It appears in any case  
488 that our results highlight the fact that the decrease in POC concentration in sediment cores  
489 should not be attributed directly to paleo-oceanographic evolution of POC fluxes at the  
490 sediment surface. Because diagenetic processes alter POC concentration, not only close to the  
491 sediment surface (Mouret et al., 2010), but also at several meters depth, buried POC  
492 represents only a transformed relict of POC exported to the sediment surface from the water  
493 column.

494

### 495         **4.3. Secondary reactions**

496

#### 497         4.3.1. Carbonate precipitation

498

499         The anoxic zone of marine sediments has been recognized as a site of carbonate  
500 precipitation because sulphate reduction and anaerobic oxidation of methane produce  
501 alkalinity (De Lange, 1986; Mucci et al., 2000; Berelson et al., 2005; Snyder et al., 2007).  
502 Carbonate precipitation can be quantified using pore water Ca<sup>2+</sup> profiles (Chatterjee et al.,  
503 2001). At all studied sites, dissolved calcium concentrations decrease with depth, suggesting  
504 that precipitation of secondary calcium carbonate may occur. Mean diffusive fluxes of  
505 dissolved calcium estimated using Fick's first law are 3.34, 1.07, 0.24, and 1.60 μmol cm<sup>-2</sup> yr<sup>-1</sup>.

506 <sup>1</sup> at stations D, B, A, and WH, respectively (Table 1), which corresponds respectively to  
507 CaCO<sub>3</sub> precipitation rates of 0.334, 0.107, 0.024, and 0.160 mg cm<sup>-2</sup> yr<sup>-1</sup>. At station B, the  
508 mean mass accumulation rate is 40 mg cm<sup>-2</sup> yr<sup>-1</sup> and carbonate minerals represent about 20%  
509 of sediments. Therefore, the rate of calcium carbonate sedimentation is 8 mg cm<sup>-2</sup> yr<sup>-1</sup>.  
510 Authigenic calcium carbonate linked to diagenetic processes represent 1.34% (0.107/8) of  
511 total carbonate in anoxic sediments. Similar calculation indicates authigenic carbonate  
512 contents of 0.4, 1.2, and 5.6% at stations D, A, and WH, respectively. These values are lower  
513 than the estimate based on a compilation of measurements of the calcium concentration of  
514 pore fluids collected at numerous seafloor sites around the globe. Authigenic carbonate  
515 precipitation accounts for at least 10% of global carbonate accumulation (Sun and Turchyn,  
516 2014). The proportions of authigenic calcium carbonate are low in the Bay of Biscay cores  
517 mostly because they are diluted in an initial high biogenic CaCO<sub>3</sub> content. In some cores, such  
518 as at station WH, the geochemical signature of fossilized calcium carbonate may be  
519 significantly contaminated by new carbonates formed during diagenesis.

520 Manganese behaviour in anoxic sediments can be influenced by carbonate chemistry  
521 (Mucci, 1988) through co-precipitation with calcium carbonates to form a rhombohedral  
522 carbonate solid solution (Middelburg et al., 1987). Dissolved manganese profiles along the  
523 Kullenberg cores show a decrease at the top of the anoxic zone of the sediments, from 10 to  
524 50 cm depth. Concentrations of manganese extracted with HCl increase slightly with depth,  
525 suggesting that dissolved Mn precipitate. At stations B, A, and WH, calculated downward  
526 diffusive fluxes of dissolved manganese correspond to accumulation rates of authigenic  
527 manganese of about 1 μmol g<sup>-1</sup> (from 0.82 to 1.25 μmol g<sup>-1</sup>), which cannot be observed in the  
528 Mn-HCl profiles because 1 μmol g<sup>-1</sup> is the error margin of the HCl extraction procedure.

529

#### 530 4.3.2. Phosphorus behaviour

531

532 Dissolved inorganic P concentrations increase with depth in the studied cores,  
533 suggesting that P included in organic matter is mineralized and released in pore water.  
534 However, the N/P ratio, as deduced from the NH<sub>4</sub><sup>+</sup>/DIP ratio, shows non-constant profiles  
535 along the cores. Values obtained at the bottom of the cores range between 50 and 200 (Fig. 5),  
536 which is far above the Redfield ratio of 16 determined for marine organic matter (Redfield et  
537 al., 1963). High N:P ratios may result from phosphate precipitation as an authigenic  
538 particulate phase. Authigenic apatite or vivianite precipitation (Ruttenberg and Berner, 1993;  
539 Dijkstra et al., 2018), or phosphorus adsorption on secondary carbonates (De Kanel and

540 Morse, 1978) are the main processes of particulate P formation in anoxic sediments. The  
541 observed increase in P-HCl with depth (from 2 to 5  $\mu\text{mol.g}^{-1}$  depending on the station; Fig. 4)  
542 points out that P authigenesis occurs here. Vivianite can be extracted with an ascorbate  
543 solution (Anschutz and Deborde, 2016), but apart from the bottom of station D core, P-Asc  
544 does not increase with depth, suggesting that P probably forms apatite or it co-precipitates  
545 with calcium carbonates (Tribovillard et al., 2010). Authigenic vivianite may be formed in the  
546 methane-rich sulphate-free layer of station D (Dijkstra et al., 2018). DIP precipitation is  
547 deduced from high  $\text{NH}_4^+$ /DIP ratio. However, we observed no decrease in DIP with depth, but  
548 an increase. This suggests that DIP precipitation rate is balanced by a higher rate of DIP  
549 production. DIP that forms authigenic phases comes from a deep source, contrary to calcium  
550 or manganese. This deep source is probably the anoxic mineralization of organic matter. DIP  
551 can also be released into the sediment pore water after reductive dissolution of P-bearing iron  
552 oxides by sulphide produced through sulphate reduction during diagenesis of buried  
553 sediments.

554

#### 555 **4.4. Anoxic diagenesis and fluxes to the ocean**

556

557 Major dissolved elements in sediment pore water, such as calcium, magnesium, and  
558 potassium, show concentration gradient due to deep sediment diagenesis (e.g. Sayles and  
559 Manheim, 1975 ; McDuff and Gieskes, 1976). Fluxes have been deduced from these gradients  
560 and have been included in the mass balance of ocean chemistry (e.g. Sayles, 1979; Sun et al.  
561 2016). Fluxes across the sediment-water interface of biogenic compounds, such as carbon,  
562 nitrogen and phosphorus, have been measured or calculated from pore water profiles in deep  
563 sea and coastal environments (Emerson and Hedges, 2003). Most of the studies on benthic  
564 biogeochemistry have been conducted on sediments lying just below the sediment water  
565 interface, since most of the organic matter is mineralized in the first centimetres of sediment.  
566 Several studies also show that sediment diagenesis far below the sediment interface feeds the  
567 surface sediment with nutrients (e.g. Schulz et al., 1994; Niewohner et al., 1998; März et al.,  
568 2008; Chong et al., 2018). Our study allows us to quantify the N-NH<sub>4</sub> and DIP fluxes that  
569 reach the sediment water interface for the 200-2000 m water depth part of the Landes Plateau.  
570 This part of the Bay of Biscay (Fig. 1) extends over 6000 km<sup>2</sup> that is covered with muddy  
571 sediment. Based on bathymetry mapping, we can consider that stations D, B, A, and WH are  
572 representative of 2%, 10%, 34%, and 54% of the Landes Plateau area. The extrapolation of  
573 the N-NH<sub>4</sub> fluxes (45, 12.5, 1.8, and 4 kmol km<sup>-2</sup> yr<sup>-1</sup> at station D, B, A, and WH,

574 respectively) to the whole Landes Plateau area, allows estimating a total weighted average  
575 flux of about 30 Mmol yr<sup>-1</sup> N-NH<sub>4</sub>. This value is low compared to N-NO<sub>3</sub> fluxes issuing from  
576 rivers that flows into the southern Bay of Biscay. For example, the flux of N-NO<sub>3</sub> from the  
577 Gironde estuary is 2700 Mmol yr<sup>-1</sup> (Anschutz et al., 2016). Nevertheless, the calculated  
578 benthic flux compares to the flux of N-NO<sub>3</sub> of the smaller Leyre River, which drains 2000  
579 km<sup>2</sup> of forest and crops. A similar calculation has been done for DIP. The flux of DIP  
580 calculated from the concentration gradient is 95, 98, 0, and 25 mol km<sup>2</sup> yr<sup>-1</sup> for station D, B,  
581 A, and WH, respectively, which gives an extrapolated flux of 151 kmol yr<sup>-1</sup> for the Landes  
582 Plateau.

583

## 584 **5. Conclusion**

585

586 Profiles of dissolved compounds involved during organic matter mineralization have  
587 been obtained from interface and Kullenberg cores at four sites of the Bay of Biscay. They  
588 indicate that biogeochemical processes of organic matter degradation occur in the buried  
589 sediments, all along the Holocene sequence, and beyond, through sulphate reduction and  
590 methane genesis. These processes favour the precipitation of secondary calcium carbonates  
591 but also authigenic forms associated to Mn and phosphorus. Fossilization of some  
592 geochemical proxies like POC, carbonates, phosphorus, or manganese, is a long-term process.  
593 Diagenetic reactions, which modifying these proxies, must be quantified in order to  
594 distinguish in a sedimentary record the part resulting from post-deposition transformations.  
595 More particularly, our results show that the decrease in POC concentration in sediment cores  
596 should not be directly attributed to paleo-oceanographic evolution of POC fluxes at the  
597 sediment surface. We show also that coatings of authigenic calcium carbonate may represent  
598 several percent of new carbonate relative to initial carbonate content, with a geochemical and  
599 isotopic signature, which may be very different of biogenic material.

600 Contribution of early diagenesis to POC loss and CaCO<sub>3</sub> authigenesis has to be  
601 estimated in paleo-oceanographic studies. Our study is based an extensive data set on 15  
602 chemical parameters measured along four sediment cores. Such long and fastidious work  
603 cannot always be done on long cores dedicated to paleo-oceanographic studies. Our results,  
604 however, suggest us to encourage the paleo-oceanographic community to follow these  
605 recommendations: bring a small bench top centrifuge during cruises to extract pore waters. In  
606 each deep-sea core collect about 20 ml sediment in a centrifuge tube at regular interval (e.g

607 every 50 cm for a 10 m long core, or a better vertical resolution if possible), extract pore  
608 water and after filtration with a syringe filter, keep the water in a fridge. This will give enough  
609 pore water to obtain profiles of dissolved calcium, sulphate and ammonium. These three  
610 parameters will allow to locate the sulphate-methane transition zone and to quantify  
611 authigenic carbonate formation and deep sediment organic matter mineralization.

612

613

614

## 615 **Acknowledgements**

616

617 This study was carried out as part of the ANR FORCLIM (ANR-05-BLAN-02751)  
618 program and was also supported financially by the project MODREGONE (Cyber-Lefe). We  
619 thank the team of the UMS ARTEMIS (CNRS-INSU-Saclay) for AMS radiocarbon  
620 measurements. The authors are grateful to the crew members of the R/V “Côte de la Manche”  
621 (CNRS-INSU) and “la Thalia” (IFREMER), and engineers of the Technical Department-  
622 INSU for their help during the sampling campaign. We also would like to thank D. Poirier, S.  
623 Bujan, and H. Derriennick for assistance during cruises, and L. Rossignol, M.H. Castera, P.  
624 Cirac and M. Crémer for support in the lab work.

625

626

## 627 **References**

628

629 Aller R.C., 1980. Diagenetic processes near the sediment-water interface of Long Island  
630 Sound. II. Fe and Mn. *Estuarine physics and chemistry : studies in Long Island Sound*,  
631 351-415.

632 Anderson L., 1979. Simultaneous spectrophotometric determination of nitrite and nitrate by  
633 flow injection analysis. *Anal. Chim. Acta* 110, 123-128.

634 Anschutz P., Zhong S., Sundby B., Mucci A, Gobeil C., 1998. Burial efficiency of phosphorus  
635 and the geochemistry of iron in continental margin sediments. *Limnol. Oceanogr.* 43  
636 (1), 53-64.

637 Anschutz P., Jorissen F.J., Chaillou G., Abu-Zaied R., Fontanier C., 2002. Recent turbidite  
638 deposition in the eastern Atlantic : early diagenesis and biotic recovery. *J. Mar. Res* 60  
639 (6), 835-854.

640 Anschutz P., Dedieu K., Desmazes F., Chaillou G., 2005. Solid speciation, oxydation state,

641 and reactivity of manganese in marine sediments. *Chem. Geol.* 281, 265-279.

642 Anschutz P. and Chaillou G., 2009. Deposition and fate of reactive Fe, Mn, P and C in  
643 suspended particulate matter in the Bay of Biscay. *Continental Shelf Research* 29 (8),  
644 1038-1043.

645 Anschutz P., Charbonnier C., Deborde J., Deirmendjian L., Poirier D., Canton M., Buquet D.,  
646 Lecroart P., 2016. Groundwater and nutrient discharge across tidal sands along the 240  
647 km-long Aquitanian coast. *Marine Chemistry* 185, 38-47.

648 Anschutz P., Deborde J., 2016. Spectrophotometric determination of phosphate in matrices  
649 from sequential leaching of sediments. *Limnology and Oceanography: Methods* 14,  
650 245-256. doi.org/10.1002:lom3.10085

651 Arndt S., Brumsack H.J., Wirtz K. W., 2006. Cretaceous black shales as active bioreactors: A  
652 biogeochemical model for the deep biosphere encountered during ODP leg 207  
653 (demerara rise). *Geochim. Cosmochim. Acta*, 70(2), 408-425.  
654 doi.org/10.1016/j.gca.2005.09.010

655 Berelson W. M., Prokopenko M., Sansone F. J., Graham A. W., McManus J., Bernhard J. M.,  
656 2005. Anaerobic diagenesis of silica and carbon in continental margin sediments:  
657 Discrete zones of TCO<sub>2</sub> production. *Geochim. Cosmochim. Acta*, 69(19), 4611-4629.  
658 doi.org/10.1016/j.gca.2005.05.011

659 Berger W.H., 1969. Ecologic patterns of living planktonic foraminifera. *Deep Sea Research*  
660 16, 1-24.

661 Berner R.A., 1980. *Early diagenesis : A Theoretical Approach*. Princeton University Press.

662 Bohrmann G., Torres M., 2006. Gas hydrates in marine sediments, in *Marine Geochemistry*,  
663 edited by H. D. Schultz and M. Zabel, pp. 481–512, Springer, Berlin.

664 Borja A., Amouroux D., Anschutz, P., Gómez-Gesteira M., Uyarra M.C., Valdés L., 2019.  
665 Chapter 5 : The Bay of Biscay. In: *World Seas: An Environmental Evaluation (Volume*  
666 *I: Europe, The Americas and West Africa)*, C. Sheppard (Editor). Elsevier, pp 113-152.

667 Borowski W. S., Paull C. K., Ussler III W., 1999. Global and local variations of interstitial  
668 sulfate gradients in deepwater, continental margin sediments: Sensitivity to underlying  
669 methane and gas hydrates. *Mar. Geol.* 159, 131–154.

670 Boudreau B.P., 1996. The diffusive tortuosity of fine-grained unlithified sediments. *Geochim.*  
671 *Cosmochim. Acta* 60, 3139– 3142.

672 Burdige D.J., 2006. *Geochemistry of marine sediments*. Princeton University Press. 1-609

673 Burdige D.J., 2011. Temperature dependence of organic matter remineralization in deeply-  
674 buried marine sediments. *Earth and Planetary Science Letters* 311, 396–410.

675 Burdige D. J., Komada T., 2013. Using ammonium pore water profiles to assess stoichiometry  
676 of deep remineralization processes in methanogenic continental margin sediments.  
677 *Geochem., Geophys., Geosyst.* 14(5), 1626–1643. doi.org/10.1002/ggge.20117

678 Burdige D.J., Komada T., Magen C., Chanton J.P., 2016. Carbon cycling in Santa Barbara  
679 Basin sediments : A modeling study. *Journal of Marine Research* 74, 133-159

680 Calvert S.E., and Pedersen T.F., 2007. Elemental Proxies for Palaeoclimatic and  
681 Palaeoceanographic Variability in Marine Sediments: Interpretation and Application”.  
682 In: C. Hillaire-Marcel and A. de Vernal, Eds., *Paleoceanography of the Late Cenozoic,*  
683 Part 1, Methods, Elsevier, New York, 2007, pp. 567-644.  
684 doi.org/10.1016/S1572-5480(07)01019-6

685 Chaillou G., Anschutz P., Lavaux G., Schäfer J., Blanc G., 2002. The distribution of U, Mo,  
686 and Cd in modern marine sediments. *Mar. Chem.* 80, 41-59.

687 Chaillou G., Schäfer J., Anschutz P., 2008. Mobility of Mo, U, As, and Sb within modern  
688 turbidites. *Marine Geology* 254 (3-4), 171-179.

689 Chatterjee S., Dickens G.R., Bhatnagar G., Chapman W.G., Dugan B., Snyder G.T., Hirasaki  
690 G.J., 2011. Pore water sulfate, alkalinity, and carbon isotope profiles in shallow  
691 sediment above marine gas hydrate systems: A numerical modeling perspective, *J.*  
692 *Geophys. Res.*, 116, B09103.

693 Chong L.S., Berelson W.M., McManus J., Rollins N.E., 2018. Meter-Scale Early Diagenesis  
694 of Organic Matter Buried Within Deep-Sea Sediments Beneath the Amazon River  
695 Plume. *Front. Mar. Sci.* 5:250. doi.org/10.3389/fmars.2018.00250

696 De Kanel, J., Morse, J. W., 1978. The chemistry of orthophosphate uptake from seawater on  
697 to calcite and aragonite. *Geochim. Cosmochim. Acta*, 42(9), 1335-1340.  
698 doi.org/10.1016/0016-7037(78)90038-8

699 De Lange, G. J., 1983. Geochemical evidence of a massive slide in the southern norwegian  
700 sea. *Nature*, 305(5933), 420-422. doi.org/10.1038/305420a0

701 De Lange G.J., 1986. Early diagenetic reactions in interbedded pelagic and turbiditic  
702 sediments in the Nares Abyssal Plain (western North Atlantic): Consequences for the  
703 composition of sediment and interstitial water. *Geochim. Cosmochim. Acta* 50, 2543-  
704 2561.

705 D'Hondt S., Jørgensen B.B., Miller D.J., Batzke A., Blake R., Cragg B.A., Cypionka H.,  
706 Dickens G.R., Ferdelman T., Hinrichs K., Holm N.G., Mitterer R., Spivack A., Wang  
707 G., Bekins B., Engelen B., Ford K., Gettemy G., Rutherford S.D., Sass H., Skilbeck  
708 C.G., Aiello I.W., Guèrin G., House C.H., Inagaki F., Meister P., Naehr T., Niitsuma

709 S., Parkes R.J., Schippers A., Smith D.C., Teske A., Wiegel J., Padilla C.N., Acosta  
710 J.L.S., 2004. Distributions of microbial activities in deep seafloor sediments.  
711 Science 306(5705), 2216-2221. doi.org/10.1126/science.1101155

712 Dickens G. R., 2001. Sulfate profiles and barium fronts in sediment on the Blake Ridge:  
713 Present and past methane fluxes through a large gas hydrate reservoir, *Geochim.*  
714 *Cosmochim. Acta*, 65, 529–543.

715 Dijkstra, N., Hagens, M., Egger, M., Slomp, C.P., 2018. Post-depositional formation of  
716 vivianite-type minerals alters sediment phosphorus records. *Biogeosciences* 15, 861–  
717 883.

718 Dittert N., Baumann K.H., Bickert T., Henrich R., Huber R., Kinkel H., Meggers H., 1999.  
719 Carbonate dissolution in the Deep-Sea : Methods, Quantification and  
720 Paleoceanographic Application. From Fischer G, Wefer G (Eds), 1999, Use of proxies  
721 in paleoceanography : examples from the South Atlantic. Springer-Verlag Berlin  
722 Heidelberg, pp 255-284.

723 Donnadiou Y., Lecroart P., Anschutz P., Bertrand P., 2002. Bias in the paleoceanographic time  
724 series: tests with a numerical model of U, C<sub>org</sub> and Al burial. *Palaeoceanography* 17, 3.  
725 doi.org/10.1029/2001PA000638

726 Dupré S., Berger L., Le Bouffant N., Scalabrin C., Bourillet J.F., 2014. Fluid emissions at the  
727 Aquitaine Shelf (Bay of Biscay, France): a biogenic origin or the expression of  
728 hydrocarbon leakage? *Cont. Shelf Res.* 88:24-33

729 Emerson S., Hedges J., 2003. Sedimentary diagenesis and benthic flux. In: Elderfield, H.,  
730 Holland, H.D., Turekian, K.K. (Eds.), *Treatise on Geochemistry*, vol. 6. pp. 293–319

731 Emiliani C., 1955. Pleistocene temperature. *J.Geol.* 63, 538-578.

732 Etcheber H., Relexans J.C., Beliard M., Weber O., Buscail R., Heussner S., 1999. Distribution  
733 and quality of sedimentary organic matter on the Aquitanian margin (Bay of Biscay).  
734 *Deep Sea Research Part II* 46, 2249-2288.

735 Eynaud F., Zaragosi S., Scourse J.D., Mojtahid M., Bourillet J.F., Hall I.R., Penaud A.,  
736 Locascio M., Reijonen A., 2007. Deglacial laminated facies on the NW European  
737 continental margin : The hydrographic significance of British-Irish Ice Sheet  
738 deglaciation and Fleuve Manche paleoriver discharges. *Geochemistry, Geophysics,*  
739 *Geosystems* 8 (6).

740 Fairbanks R.G., Mortlock R.A., Chiu T.C., Cao L., Kaplan A., Guilderson T.P., Fairbanks  
741 T.W., Bloom A.L., Grootes P.M., Nadeau M.J., 2005. Radiocarbon calibration curve  
742 spanning 0 to 50 000 years BP based on paired <sup>230</sup>Th/<sup>234</sup>U/<sup>238</sup>U and <sup>14</sup>C dates on

743 pristine corals. *Quaternary Sciences Review* 24 (16-17), 1781-1796.

744 Fontanier C., Jorissen F.J., Licari L., Alexandre A., Anschutz P., Carbonel P., 2002. Live  
745 benthic foraminiferal faunas from the Bay of Biscay : Faunal density, composition,  
746 and microhabitats. *Deep Sea Res. I*, 49, 751-785.

747 Froelich P. N., Klinkhammer G. P., Bender M. L., Luedtke N. A., Heath G. R., Cullen D.,  
748 Dauphin P., Hammond D., Hartman B., Maynard V., 1979. Early oxidation of organic  
749 matter in pelagic sediments of the eastern Atlantic: suboxic diagenesis, *Geochim.*  
750 *Cosmochim. Acta* 43, 1075-1090.

751 Ganeshram R. S., Pedersen T. F., Calvert S. E, Murray J. W., 1995. Large changes in oceanic  
752 nutrient inventories from glacial to interglacial periods. *Nature*, 376, 755-757

753 Garcia J., Mojtahid M., Howa H., Michel E., Charbonnier C., Anschutz P., Jorissen F.J.,  
754 2013. Benthic and planktic foraminifera as indicators of Late Glacial to Holocene  
755 paleoclimatic changes in a marginal environment: an example from the southeastern  
756 Bay of Biscay. *Acta Protozoologica*, 52, 163-182.

757 Garming J.F.L., Bleil U., Riedinger N., 2005. Alteration of magnetic mineralogy at the  
758 sulfate–methane transition: analysis of sediments from the Argentine continental  
759 slope. *Physics of the Earth and Planetary Interiors* 151, 290–308.

760 Hall P.O.J., Aller R.C., 1992. Rapid, small-volume, flow injection analysis for  $\Sigma\text{CO}_2$  and  
761  $\text{NH}_4^+$  in marine and freshwaters. *Limnol. Oceanogr.* 37 (5), 1113-1119.

762 Haswell S.J., 1991. *Atomic Adsorption Spectrometry, Theory, Design and Applications.*  
763 Elsevier, Amsterdam.

764 Hensen C., Zabel M., Pfeifer K., Schwenk T., Kasten S., Riedinger N., Schulz H.D., Boetius  
765 A., 2003. Control of pore-water profiles by sedimentary events and the significance of  
766 anaerobic oxidation of methane for the burial of sulfur in marine sediments. *Geochim.*  
767 *Cosmochim. Acta* 67, 2631–2647.

768 Hyacinthe C., Anschutz P., Carbonel P., Jouanneau J.M., Jorissen F.J., 2001. Early diagenetic  
769 processes in the muddy sediments of the Bay of Biscay. *Marine Geology* 177, 111-  
770 128.

771 Iversen N., Jørgensen B.B., 1985. Anaerobic methane oxidation at the sulfate-methane  
772 transition in marine sediments from the Kattegat and Skagerrak (Denmark). *Limnol.*  
773 *Oceanogr.* 30, 944–955.

774 Jouanneau J.M., Weber O., Grousset F.E., Thomas B., 1998. Pb, Zn, Cs, Sc and rare earth  
775 elements as tracers of the Loire and Gironde particles on the Bay of Biscay shelf (SW  
776 France). *Oceanologica Acta* 21, 233-241.

777 Knittel K., Boetius A., 2009. Anaerobic oxidation of methane: Progress with an unknown  
778 process. *Annu. Rev. Microbiol.* 63, 311–334.

779 La Rowe D.E., Van Cappellen P., 2011. Degradation of natural organic matter: A  
780 thermodynamic analysis. *Geochim. Cosmochim. Acta* 75 (8): 2030-2042.  
781 doi.org/10.1016/j.gca.2011.01.020

782 Martens C. S., Berner R. A., 1974. Methane production in the interstitial waters of sulfate-  
783 depleted marine sediments. *Science* 185, 1167.

784 Martinez P., Bertrand P., Calvert S.E., Pedersen T.F., Shimmield G.B., Lallier-Verges E.,  
785 Fontugne M., 2000. Spatial variations in nutrients utilization, production and  
786 diagenesis in the sediments of a coastal upwelling regime (NW Africa) : Implication  
787 for the paleoceanographic record. *Journal of Marine Research* 58, 809-835.

788 März C., Hoffmann J., Bleil U., de Lange G. J., Kasten S., 2008. Diagenetic changes of  
789 magnetic and geochemical signals by anaerobic methane oxidation in sediments of the  
790 Zambezi deep-sea fan (SW Indian ocean). *Marine Geology* 255(3-4), 118-130

791 McDuff R.E., Gieskes J.M., 1976. Calcium and magnesium profiles in DSDP waters:  
792 diffusion or reactions? *Earth Planet. Sci. Lett.* 33, 1-10

793 Middelburg J.J., De Lange G.J., Van Der Weijden C.H., 1987. Manganese solubility control in  
794 marine pore waters. *Geochim. Cosmochim. Acta* 51 (3), 759-763.

795 Migeon S., Weber O., Faugeres J.C., Saint-Paul J., 1999. SCOPIX : A new X-ray imaging  
796 system for core analysis. *Geo-Marine Letters* 18 (3), 251-255.

797 Mojtahid M., Frans J., Garcia J., Schiebel R., Michel E., Eynaud F., Gillet H., Cremer M.,  
798 Ferreira P. D., Siccha M., Howa H., 2013. High resolution Holocene record in the  
799 southeastern Bay of Biscay: global versus regional signals. *Palaeogeogr. Palaeocl.*  
800 377: 28–44

801 Mouret A., Anschutz P., Lecroart P., Chaillou G., Hyacinthe C., Deborde J., Jorissen F.J.,  
802 Deflandre B., Schmidt S., Jouanneau J.M., 2009. Benthic geochemistry of manganese  
803 in the Bay of Biscay, and sediment mass accumulation rate. *Geo-Marine Letters* 29,  
804 133-149.

805 Mouret A., Anschutz P., Deflandre B., Chaillou G., Hyacinthe C., Deborde J., Etcheber H.,  
806 Jouanneau J.M., Grémare A., Lecroart P., 2010. Oxygen and organic carbon fluxes in  
807 sediments of the Bay of Biscay. *Deep Sea Research Part I : Oceanographic research*  
808 papers 57 (4), 528-540.

809 Mouret A., Anschutz P., Deflandre B., Deborde J., Canton M., Poirier D., Grémare A., Howa  
810 H., 2016. Spatial heterogeneity of benthic biogeochemistry in two contrasted marine

811 environments (Arcachon Bay and Bay of Biscay, SW France). *Estuarine, Coastal and*  
812 *Shelf Science* 179, 51-65. doi.org/10.1016/j.ecss.2015.09.001.

813 Mucci A., 1988. Manganese uptake during calcite precipitation from sea water : conditions  
814 leading to the formation of a pseudokutnahorite. *Geochim. Cosmochim. Acta* 52,  
815 1859-1868.

816 Mucci A., Sundby B., Gehlen M., Arakaki T., Zhong S., Silverberg N., 2000. The fate of  
817 carbon in continental shelf sediments of eastern Canada : A case study. *Deep Sea*  
818 *Research Part II : Topical studies in Oceanography* 47 (3-4), 733-760.

819 Nauhaus K., A. Boetius M. Kruger, Widdel F., 2002. In vitro demonstration of anaerobic  
820 oxidation of methane coupled to sulphate reduction in sediment from a marine gas  
821 hydrate area. *Environ. Microbiol.* 4: 296–305. doi.org/10.1046/j.1462-  
822 2920.2002.00299.x

823 Niewöhner C., Hensen C., Kasten S., Zabel M., Schulz H.D., 1998. Deep sulphate reduction  
824 completely mediated by anaerobic methane oxidation in sediments of the upwelling  
825 area off Namibia. *Geochim. Cosmochim. Acta* 62, 455–464.

826 Passier H.F., Dekkers M.J., de Lange G.J., 1998. Sediment chemistry and magnetic properties  
827 in an anomalously reducing core from the eastern Mediterranean Sea. *Chemical*  
828 *Geology* 152, 287–306.

829 Pierre C., Demange J., Blanc-Valleron M.M., Dupré S. 2017. Authigenic carbonate mounds  
830 from active methane seeps on the southern Aquitaine Shelf (Bay of Biscay, France):  
831 Evidence for anaerobic oxidation of biogenic methane and submarine groundwater  
832 discharge during formation. *Cont. Shelf Res.* 133:13-25.  
833 doi.org/10.1016/j.csr.2016.12.003

834 Postma D., Jakobsen R., 1996. Redox zonation: equilibrium constraints on the Fe(III)/SO<sub>4</sub>-  
835 reduction interface. *Geochim. Cosmochim. Acta* 60 (17), 3169-3175.

836 Redfield, A. C., Ketchum, B.H., Richards, F.A., 1963. The influence of organisms on the  
837 composition of seawater. *The Sea* 2(John Wiley, New York): 26-27.

838 Reeburgh W. S., 2007. Oceanic methane biogeochemistry. *Chem. Rev.* 107, 486–513.

839 Reichart G.J., Schenau S.J., De Lange G.J., Zachariasse W.J., 2002. Synchronicity of oxygen  
840 minimum zone intensity on the Oman and Pakistan Margins at sub-Milankovitch time  
841 scales. *Mar .Geol.* 185 (3-4), 403-415.

842 Ruffine L., Donval J.P., Croguennec C., Bignon L., Birot D., Battani A., Bayon G., Caprais  
843 J.C., Lantéri N., Levaché D., Dupré S., 2017. Gas Seepage along the Edge of the  
844 Aquitaine Shelf (France): Origin and Local Fluxes. *Geofluids* 2017:13

845 Ruppel C.D., Kessler J.D., 2017. The interaction of climate change and methane hydrates.  
846 *Reviews of Geophysics* 55 (1), 126-168

847 Ruttenberg K.C., 1992. Development of a sequential extraction method for different forms of  
848 phosphorus in marine sediments. *Limnol. Oceanogr.* 37 (7), 1460-1482.

849 Ruttenberg K.C., Berner R.A., 1993. Authigenic apatite formation and burial in sediments  
850 from non-upwelling, continental margin environments. *Geochim. Cosmochim. Acta* 57  
851 (5), 991-1007.

852 Sayles F.L., Manheim F.T., 1975. Interstitial solutions and diagenesis in deeply buried marine  
853 sediments. *Geochim. Cosmochim. Acta* 39, 103-128

854 Sayles F.L., 1979. The composition and diagenesis of interstitial solutions—I. Fluxes across  
855 the seawater-sediment interface in the Atlantic Ocean. *Geochim. Cosmochim. Acta* 43,  
856 1–19.

857 Schiebel R., Waniek J., Bork M., Hemleben C., 2001. Planktic foraminiferal production  
858 stimulated by chlorophyll redistribution and entrainment of nutrients. *Deep Sea*  
859 *Research part I* 48, 721-740.

860 Schmidt S., Jouanneau J.M., Weber O., Lecroart P., Radakovitch O., Gilbert F., Jézéquel D.,  
861 2007. Sedimentary processes in the Thau lagoon (France) : from seasonal to century  
862 time scales. *Estuarine, coastal and shelf science* 72 (3), 534-542.

863 Schmidt S., Howa H., Mouret A., Lombard F., Anschutz P., Labeyrie L., 2009. Particle fluxes  
864 and recent sediment accumulation on the Aquitanian margin of Bay of Biscay.  
865 *Continental Shelf Research* 29, 1044-1052.

866 Schulz H.D., Dahmke A., Schinzel U., Wallmann K., Zabel, M., 1994. Early diagenetic  
867 processes, fluxes and reaction rates in sediments of the South Atlantic. *Geochim.*  
868 *Cosmochim. Acta* 58, 2041-2060.

869 Schultz H.D., Zabel M., 2006. *Marine Geochemistry*. Springer-Verlag, Berlin, Heidelberg, 2<sup>nd</sup>  
870 edition.

871 Snyder G. T., Hiruta A., Matsumoto R., Dickens G.R., Tomaru H., Takeuchi R., Komatsubara  
872 J., Ishida Y., Yu H., 2007. Pore water profiles and authigenic mineralization in shallow  
873 marine sediments above the methane-charged system on Umitaka Spur, Japan Sea.  
874 *Deep-Sea Res. II* 54, 1216–1239.

875 Soetaert, K., Herman, P. M. J., and Middelburg, J. J., 2006. A model of early diagenetic  
876 processes from the shelf to abyssal depths. *Geochim. Cosmochim. Acta*, **60**: 1019-  
877 1040

878 Stookey L.L., 1970. Ferrozine – a new spectrophotometric reagent for iron. *Anal. Chem.* 42,

879           779-781.

880 Sun X., Turchyn A. V., 2014. Significant contribution of authigenic carbonate to marine  
881           carbon burial. *Nature Geoscience*, 7(3), 201-204. doi.org/10.1038/ngeo2070

882 Sun X., Higgins J., Turchyn, A.V., 2016. Diffusive cation fluxes in deep-sea sediments and  
883           insight into the global geochemical cycles of calcium, magnesium, sodium and  
884           potassium. *Marine Geology* 373, 64-77

885 Sundby B., Lecroart P., Anschutz P., Katsev S., Mucci A., 2015. When deep diagenesis in  
886           Arctic Ocean sediments compromises manganese-based geochronology. *Marine*  
887           *Geology* 366, 62-68. doi.org/10.1016/j.margeo.2015.04.005

888 Treude T., Krause S., Maltby J., Dale A. W., Coffin R., Hamdan L. J., 2014. Sulfate reduction  
889           and methane oxidation activity below the sulfate-methane transition zone in alaskan  
890           beaufort sea continental margin sediments: Implications for deep sulfur cycling.  
891           *Geochim. Cosmochim. Acta* 144, 217-237. doi.org/10.1016/j.gca.2014.08.018

892 Tribovillard N., Récourt, P, Trentesaux A., 2010, Bacterial calcification as a possible trigger  
893           for francolite precipitation under sulfidic conditions, *Comptes Rendus Geoscience*  
894           342, 27-35

895 Wefer G., Berger W.H., Bijma J., Fisher G., 1999. Use of proxies in paleoceanography -  
896           Examples from the South Atlantic. In : Fisher G., Wefer G. (Eds.), *Clues to ocean*  
897           *history : a brief overview of proxies*. Springer, Berlin, Heidelberg, pp. 1-68.

898

899

900

901

902

903

904

905

906 **Figure captions**

907

908 Figure 1: Bathymetric map of the southern part of the Bay of Biscay and location of stations  
909 (St) where sediment cores were sampled

910

911 Figure 2: Vertical profiles of sediment properties at the 4 studied stations: porosity (%),  
912 median grain size (D50 in  $\mu\text{m}$ ),  $^{14}\text{C}$  dating in cores B, A, and WH in calendar years BP, and  
913  $^{210}\text{Pb}_{\text{xs}}$  and  $^{137}\text{Cs}$  profiles in gravity and interface cores of station D.

914

915 Figure 3: Vertical profiles of particulate organic carbon concentration (POC in dry weight %),  
916  $\text{CaCO}_3$  in dw% calculated from particulate inorganic carbon concentration, and total  
917 particulate sulphur (TS, in  $\mu\text{mol g}^{-1}$ ) at the 4 stations. Profiles have been drawn from data  
918 obtained on long gravity cores, and from averaged profiles obtained from interface cores  
919 (surf) collected between 1998 and 2006.

920

921 Figure 4 : Vertical profiles of particulate P, Fe, and Mn obtained after leaching with an  
922 ascorbate (Asc) solution and a 1-N HCl solution. Profiles have been drawn from data obtained  
923 on long gravity cores, and from averaged profiles obtained from interface cores (surf)  
924 collected between 1998 and 2006. Note the change in concentration scale for Fe and Mn at  
925 station WH.

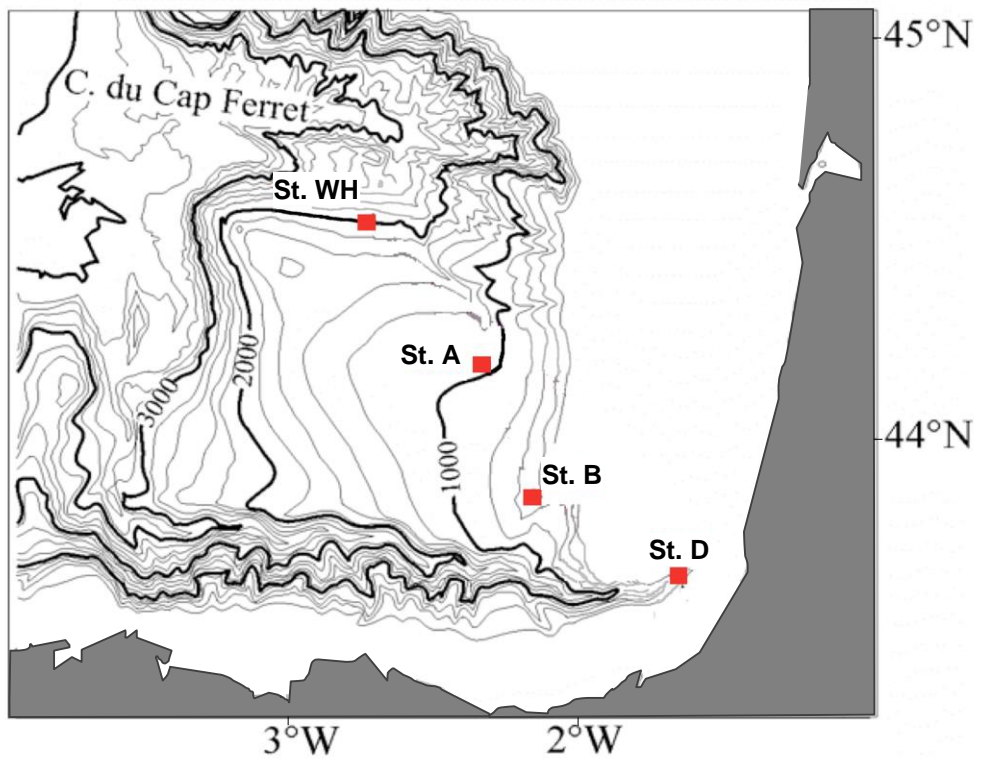
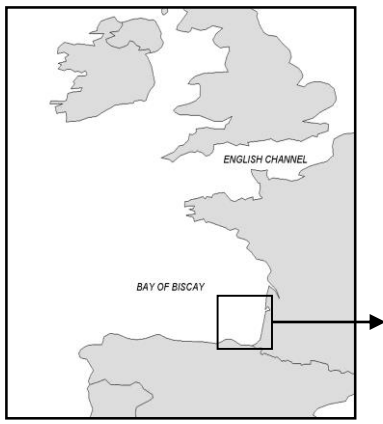
926

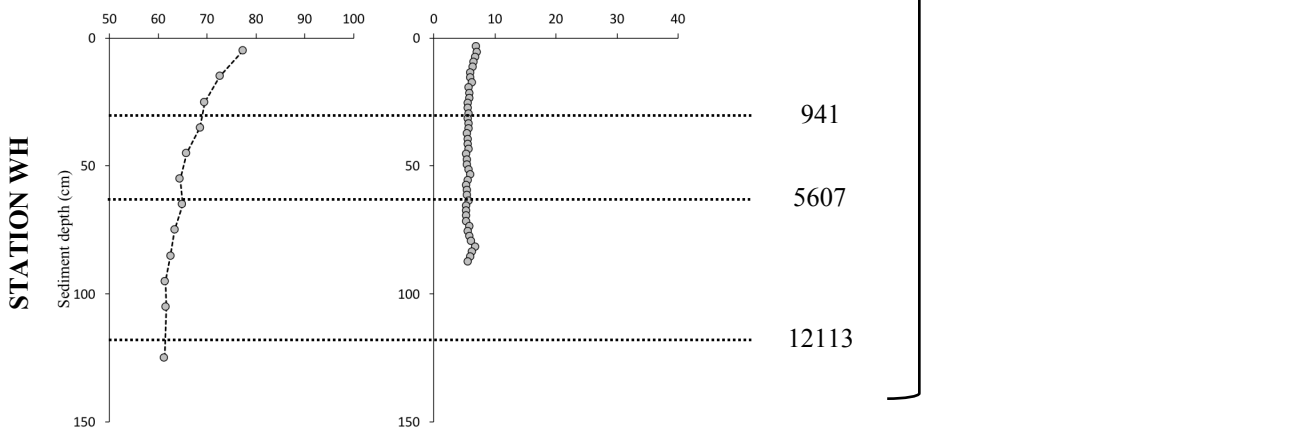
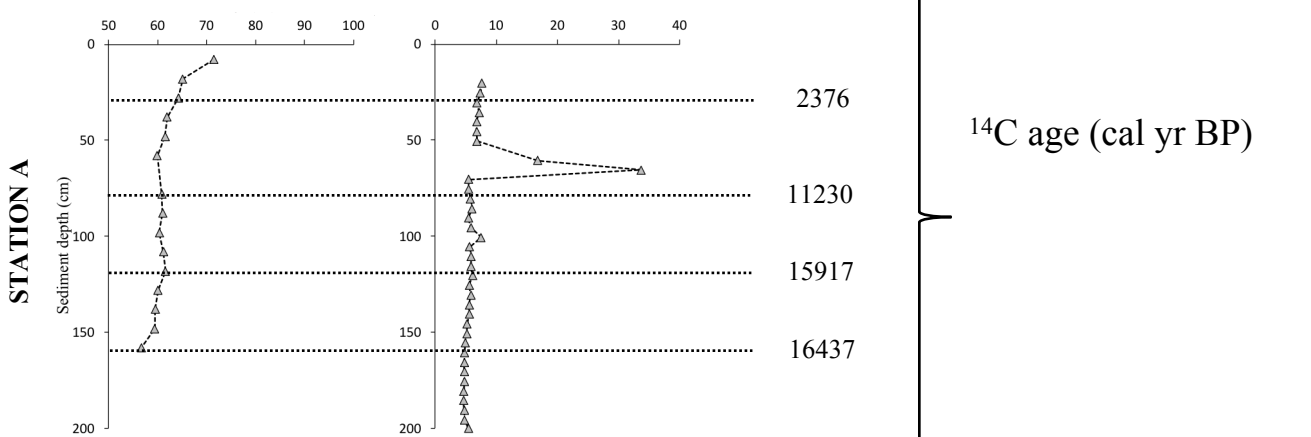
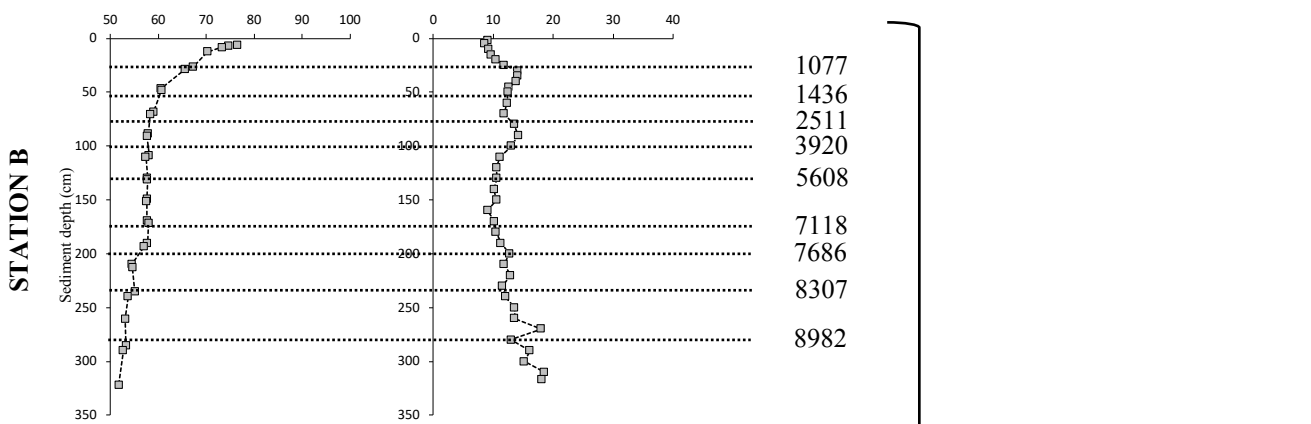
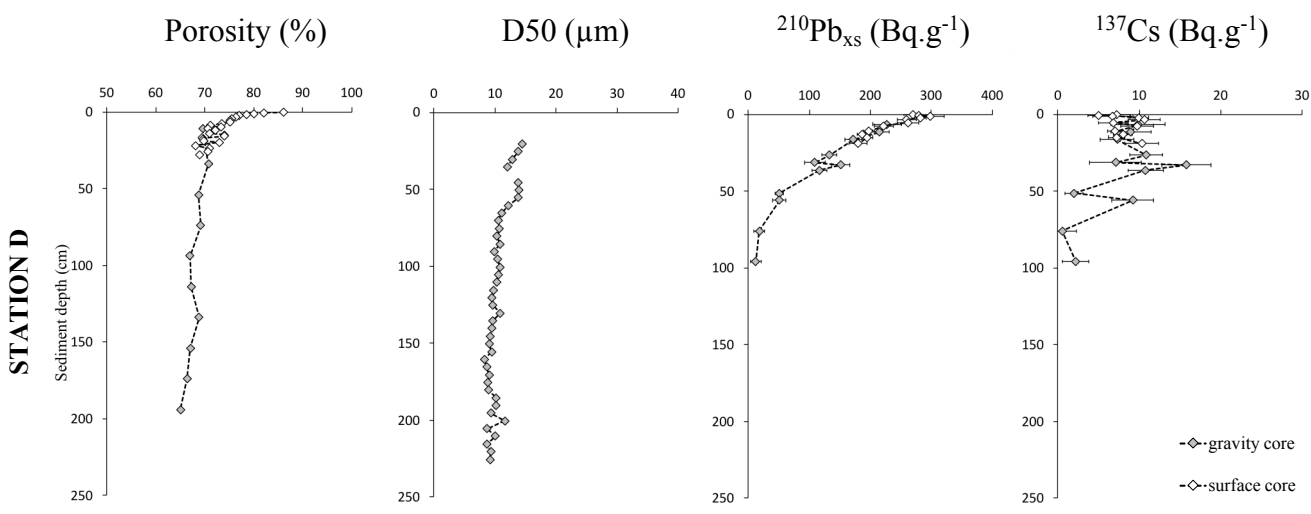
927 Figure 5 : Vertical profiles of dissolved nitrate, ammonium, inorganic phosphorus (DIP),  
928  $\text{NH}_4^+$ /DIP ratio, methane, Fe and Mn, sulphate, calcium, and dissolved inorganic carbon  
929 (DIC) in sediment core pore waters. Profiles have been drawn from data obtained on long  
930 gravity cores, and from averaged profiles obtained from interface cores (surf) collected  
931 between 1998 and 2006.

932

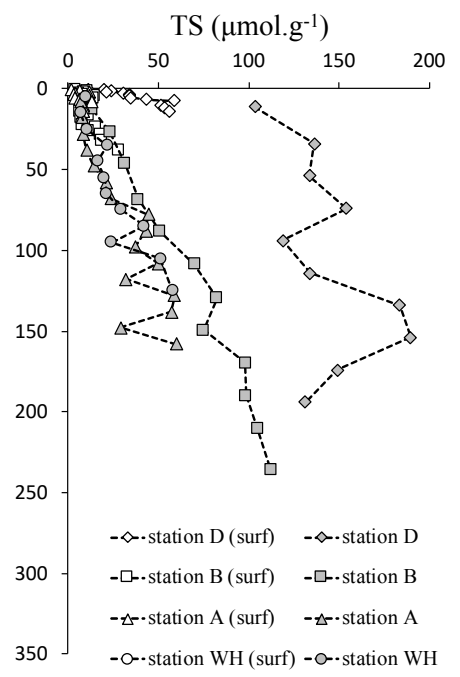
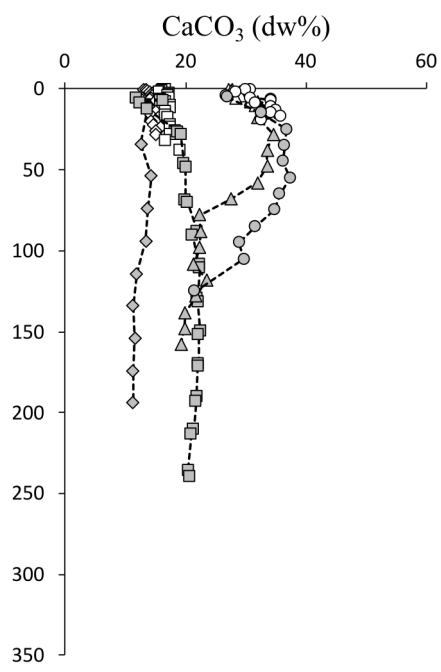
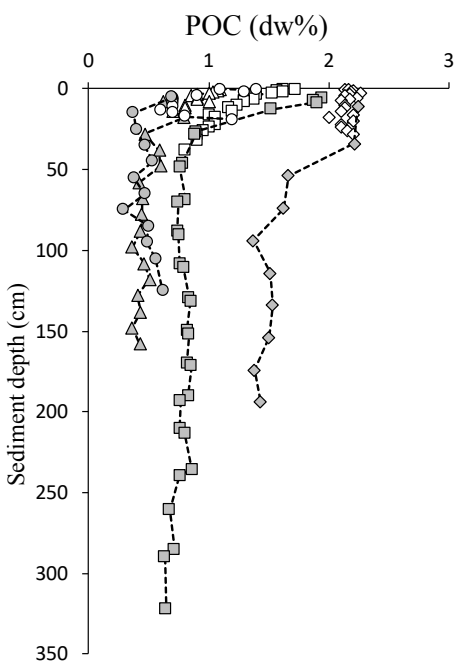
933

934

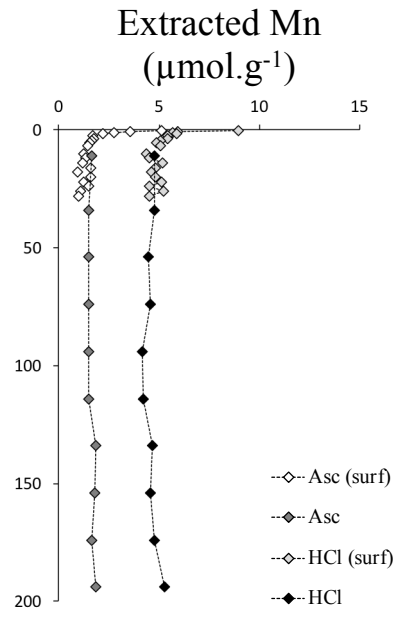
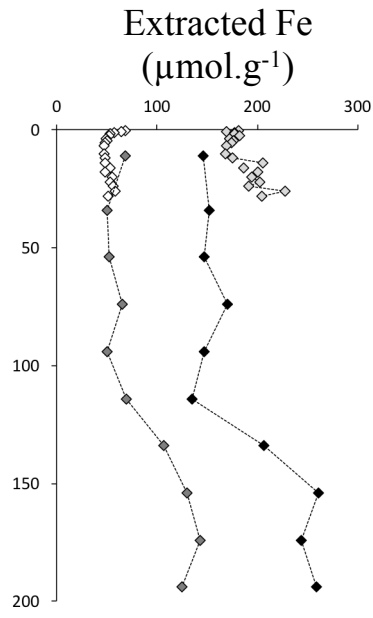
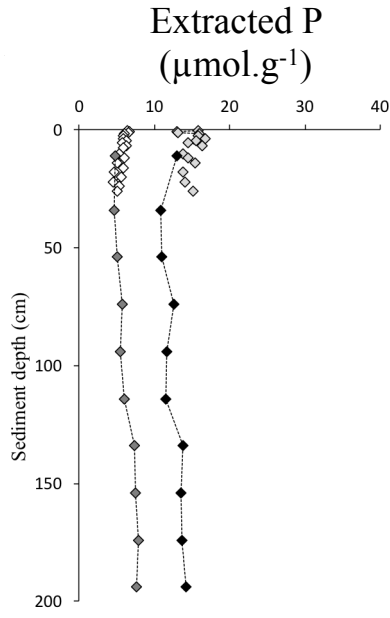




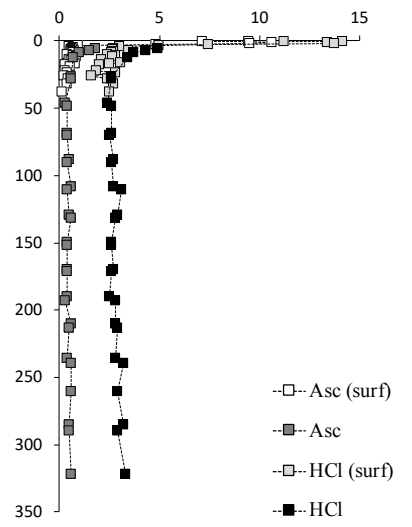
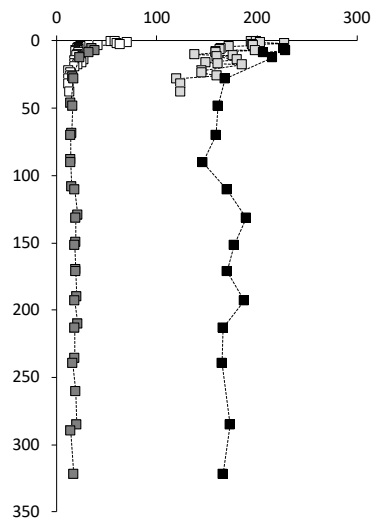
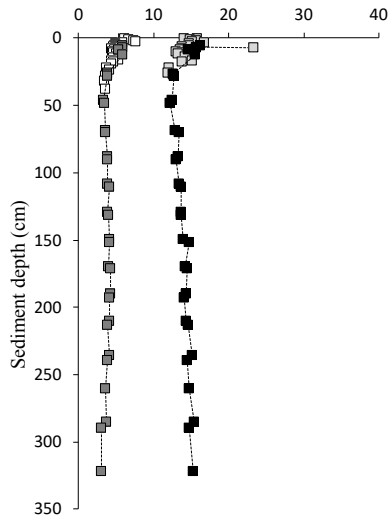
$^{14}\text{C}$  age (cal yr BP)



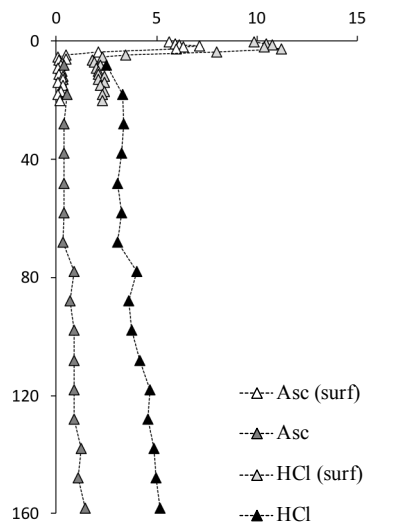
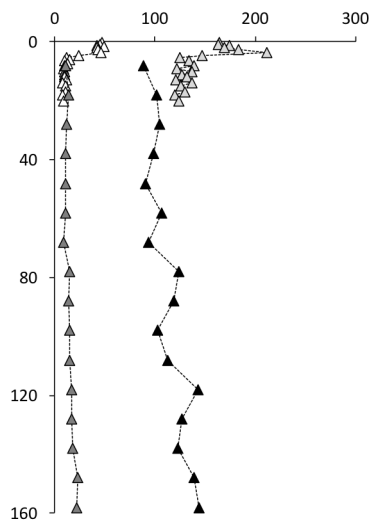
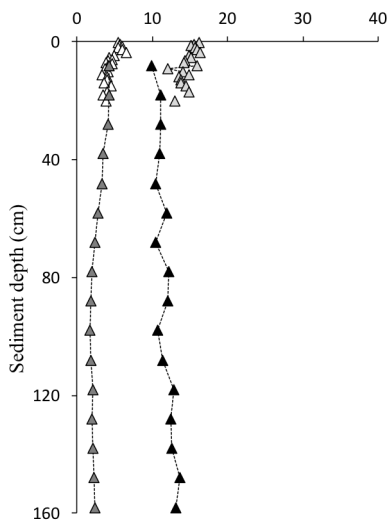
STATION D



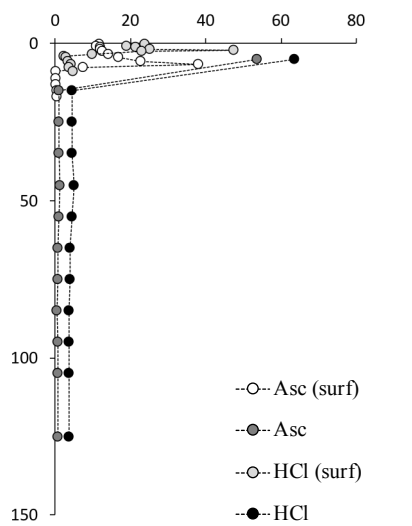
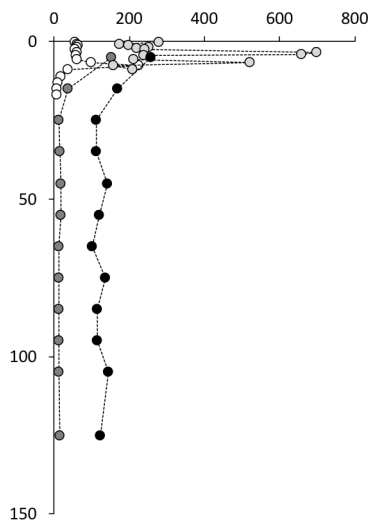
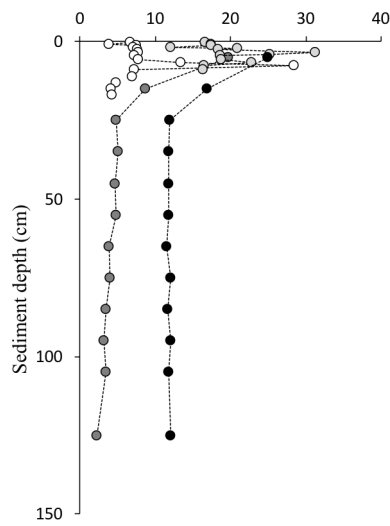
STATION B

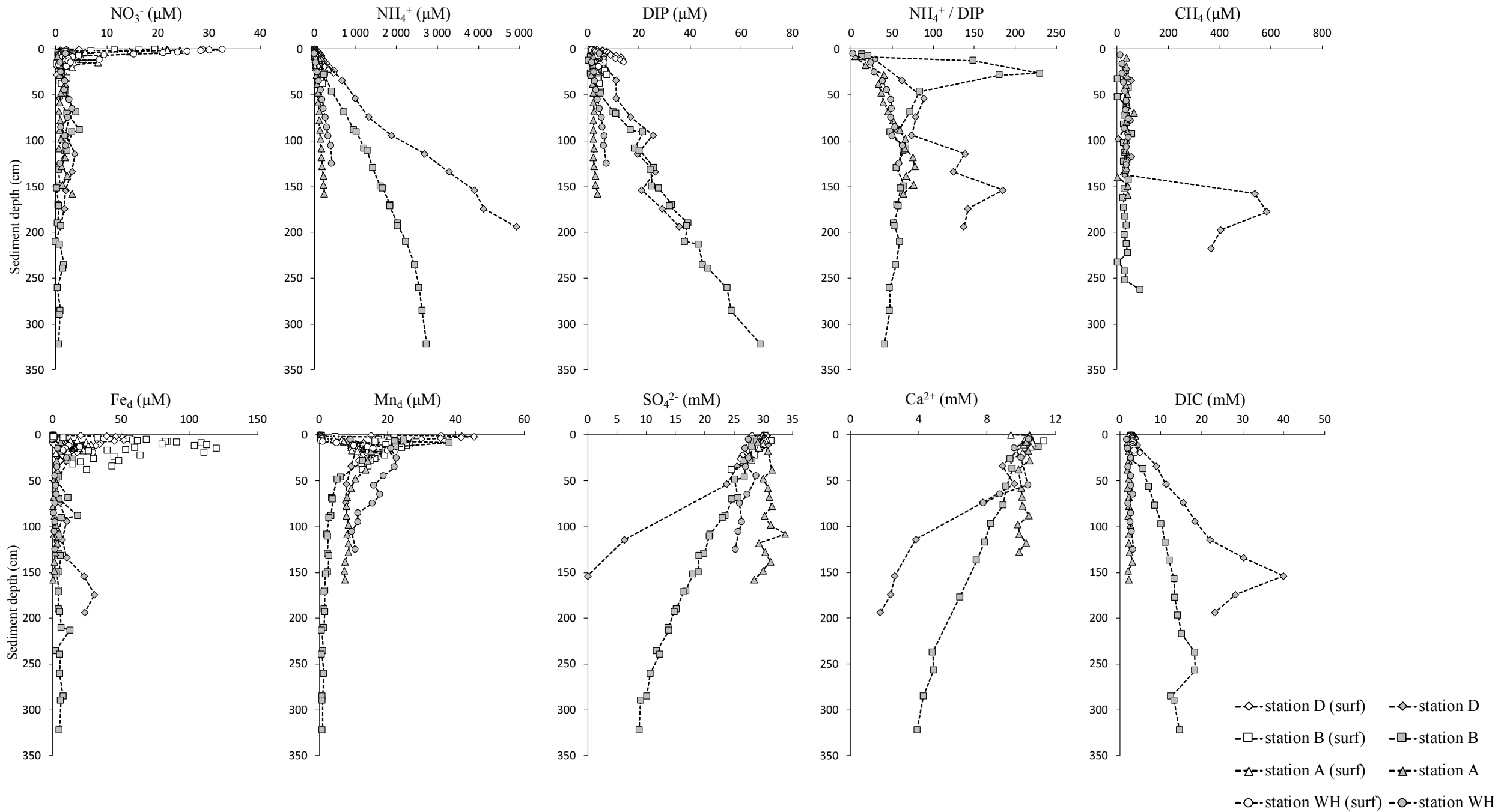


STATION A



STATION WH





1 Table 1 : Diffusive fluxes (in  $\mu\text{mol cm}^{-2} \text{ yr}^{-1}$ ) of sulphate, ammonium, calcium, and phosphate  
 2 dissolved in sediment core pore waters.  $D_s$  (in  $\text{cm}^2 \text{ s}^{-1}$ ) is the diffusion coefficient calculated  
 3 from tracer diffusion coefficient in seawater after Schulz and Zabel (2006) and porosity  
 4 according to [Boudreau \(1996\)](#). The diffusive coefficient of  $\text{HPO}_4^{2-}$  has been chosen to  
 5 represent the flux of dissolved inorganic phosphorus.  
 6

Station	Depth (m)	T (°C)	Porosity	$\text{SO}_4^{2-}$		$\text{NH}_4^+$		$\text{Ca}^{2+}$		$\text{HPO}_4^{2-}$	
				$D_s$	flux	$D_s$	flux	$D_s$	flux	$D_s$	flux
D	140	12	0.67	4.00E-10	18.1	7.56E-10	4.49	3.01E-10	3.34	2.82E-10	0.0095
B	550	11	0.58	3.35E-10	4.26	6.34E-10	1.25	2.51E-10	1.07	2.35E-10	0.0098
A	1000	10	0.61	3.41E-10	0.48	6.49E-10	0.18	2.56E-10	0.24	2.39E-10	\
WH	2000	4	0.63	2.86E-10	1.26	5.51E-10	0.41	2.13E-10	1.60	1.96E-10	0.0025

7  
 8  
 9  
 10  
 11